Utrecht University

Master Thesis

The Amundsen Sea Low: variability in present and future climates

Author:
F.Y.J. (Freerk) Drijfhout (4009509)

Supervisors:
Prof. Dr. M.R. (Michiel) van den Broeke
Dr. L. (Leo) van Kampenhout

December 13, 2021

Universiteit Utrecht

Abstract

The Amundsen Sea Low (ASL) is a semi-permanent climatological low pressure system, located in the Southern Pacific Ocean, close to the West Antarctic Ice Sheet. It is an important regulator of West Antarctic and Antarctic Peninsula climate with the potential to accelerate future ice-loss, by driving atmosphere and ocean circulations. Using ERA5-reanalysis data, we develop an ASL climatology, investigating variability in both depth and location on different timescales. We find that the depth of the ASL is influenced by the two large-scale modes of atmospheric variability on the Southern Hemisphere: The Southern Annular Mode (SAM) and El Niño Southern Oscillation (ENSO). Our results show that the combination of SAM+ (SAM-) and La Niña (El Niño) cause negative (positive) pressure anomalies in the Amundsen Sea, while other combinations show significantly reduced effects. The zonal location of the ASL is linked to the mid-tropospheric planetary waves, causing a 60° eastward shift during austral summer compared to other seasons. The synoptic scale atmospheric patterns in the Amundsen-Bellingshausen and Ross Seas are dominated by the ASL. The advection of both warm air (to the east) and cool air (to the west) around the ASL influences the climate of West Antarctica and the Antarctic Peninsula, creating large anomalies in temperature, precipitation and sea ice. Using the Community Earth System Model (CESM2), we are able to asses future ASL variability and its influence on the AIS, comparing a historical (1979-2014) and future period (2065-2100). The modelled ASL in CESM2 matches the observations from ERA5 well. We show that the future ASL will likely deepen as a consequence of anthropogenic forcing, further spatially extending its influence on near-surface wind patterns over parts of East Antarctica. While in present day climate an anomalously strong ASL has a net cooling effect on Antarctica, in the future the area of warming response increases, especially during summer and autumn.

Contents

1 Introduction

The Antarctic Ice Sheet (AIS) holds the vast majority of land ice on Earth, which makes the AIS potentially the largest contributor to future global sea level rise. Future projections, however, show a broad uncertainty range in this contribution. This large uncertainty makes it crucial to develop a better understanding of the different processes that influence the Antarctic mass balance, such as precipitation, sea ice cover, temperature and wind.

Globally, the lowest mean sea level pressure (MSLP) values are found in the Antarctic circumpolar trough (ACT), around 65° S (Figure 1). This band of low pressure around Antarctica arises after climatological averaging (here 36-year seasonal means) and plays an important role in the extra-tropical Southern Hemisphere (SH) circulation (Goyal et al., 2021a; Hosking et al., 2016). The ACT shows very distinctive seasonal variations, linked to the southern semiannual oscillation (SAO)[1] (Van den Broeke, 2000; Fogt et al., 2012). The SAO describes the twice-yearly contraction and expansion of the ACT as a response to the twice-yearly intensification of the meridional temperature gradient. This contraction and expansion affects the ACT, which is deeper during austral spring (September, October, November) and autumn (March, April, May). Zonally within the ACT, three major low pressure systems can be distinguished (Figure 2a), reflecting the zonal wave number 3 (ZW3) circulation around Antarctica (Goyal et al., 2021a; Raphael, 2004; Turner et al., 2013). The strongest of these three climatological low pressure systems, located in the Southern Pacific Ocean is generally referred to as the Amundsen Sea Low (ASL).

[1]We write southern SAO here to contrast it from the equatorial SAO. Henceforth, we will simply use SAO when the southern SAO is implied.

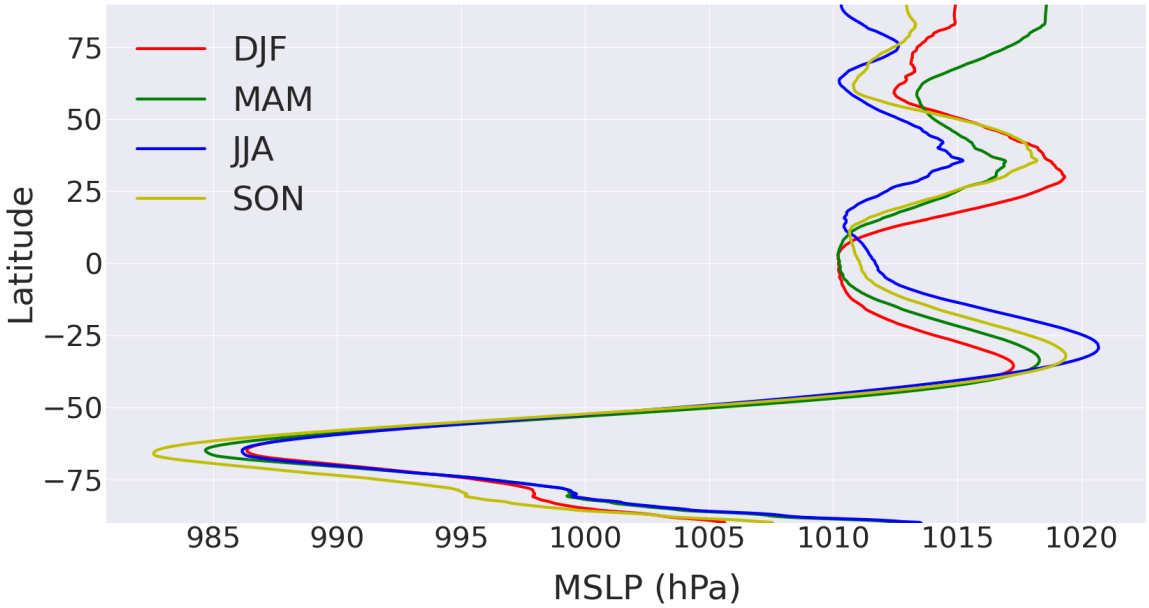

Figure 1: Zonal mean sea level pressure (MSLP) per latitude. Different colors show the three-monthly mean seasonal differences. Remarkable is the large asymmetry between the Northern Hemisphere (NH) and Southern Hemisphere (SH), which can be ascribed to the differences in land cover and the formation of strong high pressure over the NH continents in winter. Because of the isolation of Antarctica, a deep circumpolar trough can only exist on the SH. DJF: December, January, February; MAM: March, April, May; JJA: June, July, August; SON: September, October, November. Data from ERA5-reanalysis, 1979-2014.

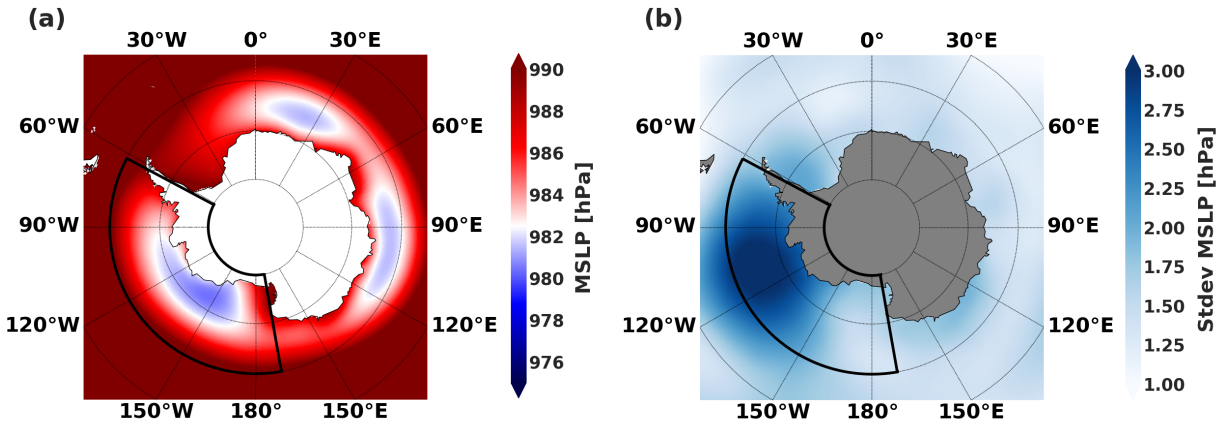

Figure 2: (a) Yearly MSLP for the high SH latitudes. Three major low pressure systems can be distinguished, reflecting the zonal wave number 3 (ZW3) circulation around Antarctica. The Amundsen Sea Low (ASL) is located in the black box, bounded by 60°-80° S and 170°-298° E. (b) Same as for (a), but here the standard deviation (stdev) for MSLP is plotted. Stdev values in the ASL region are higher than anywhere else in the SH, hence this region is called "the pole of variability". Data from ERA5-reanalysis, 1979-2014.

The ASL is a semi-permanent low pressure system in the Amundsen-Bellingshausen and Ross Seas, zonally bounded by the Antarctic Peninsula in the east (298° E) and the Transantarctic Mountains in the west (170° E) , (Hosking et al., 2016; Coggins and McDonald, 2015). It experiences a large seasonal cycle in both depth and location and this region is therefore often called "the pole of variability" , (Goyal et al., 2021b; Lachlan-Cope et al., 2001). As a result, the ASL-MSLP standard deviation (stdev) is the highest in the SH (Figure 2b).

Variation in both location and depth of the ASL have significant impacts on the West Antarctic climate (Clem et al., 2017; Coggins and McDonald, 2015; Raphael et al., 2016). Consistent with a low-pressure system in the SH, a dominant northerly flow exists east of the ASL, transporting relatively warm and humid air over parts of West Antarctica and the Antarctic Peninsula (AP). West of the ASL, a southerly flow causes relatively cold and dry conditions and drives large amounts of sea ice to flow northwards into the Ross Sea. Because of its high variability, these flow conditions around the ASL change not only on synoptic timescales, but also on both interseasonal and interannual timescales. For instance during austral summer, the ASL has a more eastern location (270° E), reducing its influence on the Ross Ice Shelf compared to other seasons (210° E), (Cohen et al., 2013; Coggins and McDonald, 2015). Furthermore, changes in the ASL's absolute depth affect the strength of surface wind patterns in the surrounding area. A strong (weak) ASL causes a strong (weak) northerly flow down the AP, which in turn leads to increased (decreased) precipitation and decreased (increased) sea ice extent in this area (Turner et al., 2013).

The link with ZW3 explains a large fraction of the ASL's longitudinal movement during the year (Turner et al., 2013; Coggins and McDonald, 2015). Previously, it has been suggested that the existence of three climatological low pressure systems around Antarctica was a result of the presence of three major landmasses and oceans in the SH (Yuan and Li, 2008; Raphael and Hobbs, 2014). However, a study by Goyal et al. (2021a) shows that low level flow perturbations in the tropics are the source of this ZW3 pattern. These perturbations act as a Rossby wave train that flow poleward and eastward from the source region. The lowest wavenumbers (k=1,2,3) have the strongest meridional group velocity and therefore can travel the furthest poleward. Wavenumber 3 is the dominant wavenumber in the region 50° - 65° S, which explains the dominant ZW3 feature that exists in this area. The location of the largest and strongest of

the three climatological low pressures systems over the Amundsen Sea is explained by another mechanism. Goyal et al. (2021b) shows that the location and depth of the ASL is solely a result of the interaction between Antarctic topography and the westerly wind jet, with tropical teleconnections playing a minor role. The presence of high topography on both sides (Antarctandes in the east and Transantarctic Mountains in the west) of the Amundsen-Bellingshausen and Ross Seas causes the ASL to be trapped between those two mountain ridges.

ASL variability, however, is largely affected by tropical teleconnections (Ding et al., 2014; Scott Yiu and Maycock, 2019; Goyal et al., 2021a), in which the El Niño Southern Oscillation (ENSO) holds strong correlations to high latitude atmospheric circulation patterns. In the literature, ASL variability in depth and location as well as trends have been linked with large scale atmospheric oscillations, such as ENSO and the Southern Annular Mode (SAM), (Fogt and Marshall, 2020; Pope et al., 2017; Goyal et al., 2021a; Maclennan and Lenaerts, 2021; Clem et al., 2017). The combination of different SAM and ENSO phases show in some cases a strong amplification of pressure anomalies in the ASL region. In other combinations this signal is severely reduced or completely absent.

A number of recent studies have found significant deepening trends of the ASL during austral summer, linked with the loss of stratospheric ozone (England et al., 2016; Fogt and Zbacnik, 2014; Goyal et al., 2021b). Although the ozone hole is a feature of austral spring, the resultant changes in atmospheric circulation show a time-lag with the largest impacts during the subsequent season (Turner et al., 2013). This summer deepening is also visible in the SAM, holding strong correlations with the ASL and driven primarily by ozone depletion, with increasing greenhouse gas (GHG) concentrations playing only a minor role (England et al., 2016; Raphael et al., 2016). However, with the projected recovery of the ozone hole, future trends in both ASL and SAM are expected to be dominated by changes in GHG concentrations (Goyal et al., 2021b; Raphael et al., 2016). The relative coupling strengths between stratospheric ozone depletion, increasing GHG concentrations and the observed current and future ASL trends remain a subject of debate. Large variability in sea level pressure (SLP) and the relatively short period of observations make it difficult to distinguish whether these trends are the result of climate drivers or fall within the range of natural variability (Hosking et al., 2016).

The aim of this thesis is to investigate the climatological ASL, its variability in present and future climates, and its impact on sea ice, temperature and precipitation in the Antarctic region. First, we analyse and interpret the present mean state of the climatological ASL using ERA5-reanalysis data and elucidate possible differences with previous descriptions using older and less detailed reanalysis products (NCEP, ERA-Interim). Secondly, we investigate the correlation between the ASL and the two largest atmospheric oscillations in the SH: SAM and ENSO. Thirdly, we assess relations between ASL variability and variations in sea ice extent, precipitation over West Antarctica and temperature in the region. For all these cases, we additionally assess ASL representation in the Community Earth System Model 2 (CESM2) by comparing to ERA5-reanalysis data for the same period (1979-2014). As a final step, we study the response of the ASL to a future (2015-2100) shared socio-economic pathways (SSP5-8.5) scenario from the intergovernmental panel on climate change (IPCC) (Ebi et al., 2014), using ensemble runs of CESM2.

This thesis is laid out as follows: Section 2 provides an overview of the data and methods used. The climatological characteristics and variability of the ASL are examined in Section 3. Section 4 describes the correlation of the ASL with SAM and ENSO. In Section 5, the ASL's influence on the Antarctic climate is investigated. Section 6 provides the results for the future. A summary and conclusion are given in Section 7 and finally limitations and directions for future research are discussed in Section 8.

2 Data and Methods

2.1 Observational data from ERA5

For this study, we analyse the atmospheric and oceanic fields of the ERA5-reanalysis dataset from the European Center of Medium-Range Weather Forecasts (ECMWF), (Hersbach et al., 2020). ERA5 is the fifth generation ECMWF atmospheric reanalysis of the global climate, produced in 2019, available on both single levels and pressure levels. It has shown to be an excellent representation of high SH latitude climate (Tetzner et al., 2019; Zhu et al., 2021). ERA5 has a grid resolution of 0.25° latitude by 0.25° longitude, equivalent to ∼28 km by ∼10 km at the location of the ASL. Although this study is conducted in 2021, we specifically chose to analyse the period 1979-2014, because our aim is to compare ERA5 at a later stage with CESM2, for which the historical period ends in 2014. CESM2 data from 2015 onwards is not unambiguous, but depends on a chosen SSP scenario, hence is not valid for comparison to ERA5-reanalysis. Strictly speaking, ERA5 is not an observational data set, but model generated data in a set up where the model is assimilating observations[2].

The main variable of interest to analyse the climatological ASL is SLP, which is studied on different temporal resolutions: daily, monthly, seasonal and yearly. The daily analysis is performed with ERA5 hourly mean data; the monthly, seasonal and yearly analysis is performed with ERA5 monthly mean data. The seasonal analysis has been conducted based on the austral seasons: summer (December, January, February), autumn (March, April, May), winter (June, July, August) and spring (September, October, November), denoted with DJF, MAM, JJA and SON respectively. Apart from SLP, we study the following single-level variables: sea surface temperature (SST), sea ice extent (SIE), 2-meter temperature (T2M) and total precipitation (TP); along with a study of different pressure levels: the geopotential height field at 250 hPa (Z250), 500 hPa (Z500) and 750 hPa (Z750). For all these different fields, we restricted our analysis to the SH, with the exception of SST, for which we examine data between 30° N and 90° S. Furthermore, the SLP analysis has been performed with masked out land points, as they are not representative over the high orography of Antarctica (Hosking et al., 2016).

2.2 Model data from CESM2

We also use output from CESM2, released in 2018, which took part in the Coupled Model Intercomparison Project phase 6 (CMIP6), (Danabasoglu et al., 2020). CESM2 is a fully-coupled, global climate model that provides state-of-the-art computer simulations of the Earth's past and future climate states. For the purpose of model evaluation, we analyse the same variables with CESM2 as from the ERA5-reanalysis data: SLP, SST, T2M, TP, SIE, Z250, Z500 and Z750, on seasonal timescales for the period 1979-2014. After evaluation, we analyse the response of the ASL in CESM2 for a future period (2015-2100), using the SSP5-8.5 scenario from the IPCC sixth assessment report (AR6). Future trends and patterns in both the ASL and the SAM are easier to detect using the extreme SSP5-8.5 scenario compared to more moderate GHG emission pathways, which is especially important in the ASL region because of the large natural variability that exists here. All calculations have been performed using one member for both the historical (1979-2014) and future period (2015-2100). We validated that this member is a good representation of a multi-member mean, using a small ensemble with 3 members.

[2]Henceforth, we will often refer to ERA5 as "observations" and to CESM2 as "model".

CESM2 uses a spatial resolution of ∼0.94° latitude by 1.25° longitude, equivalent to ∼105 km by ∼48 km at the location of the ASL. The motivation for using a relatively coarse-resolution global climate model instead of a finer-resolution regional climate model is that part of this study focuses on the tropical teleconnections between the ASL and ENSO. A finer-resolution regional climate model (such as RACMO2) would probably more accurately represent the different variables (SIE, T2M, TP) over Antarctica. However, it would not be able to show relations between the ASL and lower latitude modes, such as SAM and ENSO.

2.3 Capturing the ASL

There is some disagreement on the optimal method for capturing the depth of the ASL (i.e., former studies differ in their choice of the region examined). Turner et al. (2013) chose their region in such a way that it included the complete Antarctic Peninsula, but not all of the Ross Sea. Raphael et al. (2016) and Coggins and McDonald (2015) included the complete Ross Sea in their region, but excluded the Antarctic Peninsula. A recent study (Goyal et al., 2021b) shows that the location of the ASL is largely constrained by Antarctic topography and therefore trapped between the Transantarctic Mountains in the west (170° E) and the Antarctandes in the east (298° E). Hence, we chose the zonal boundaries of our region to be on these topographic margins and created a box to capture the ASL, bounded by 60°-80° S and 170°-298° E (shown in Figure 2), a definition also used by Hosking et al. (2016).

Our method of defining the exact location of the ASL consist of finding the grid-cell with the lowest value for SLP in this box. As a first step, we calculate the temporal mean of a certain month or season for the period 1979-2014. Subsequently, we locate the grid-cell with the lowest SLP value and define that cell as the center location of the ASL during that particular month or season. Hosking et al. (2013) argues that capturing the minimum relative MSLP (RMSLP) is a superior method, as it represents air pressure gradients that drive surface winds. The RMSLP is calculated by subtracting the zonal mean SLP from the absolute sea level pressure field. However, using the RMSLP excludes influences from the SAM and SAO and does not show the clear seasonality of the ASL. Furthermore, a study by Coggins and McDonald (2015) shows that the use of the absolute MSLP instead of the RMSLP results in a more distinctive spatial response of the ASL.

2.4 Computing indices for ASL, SAM and ENSO

Apart from defining a monthly or seasonal mean depth and location of the ASL over a larger period of time, we compute an ASL-index. The ASL-index is calculated in the same way, by finding the monthly or seasonal grid cell with the lowest value for SLP. However, in this case we do not compute the temporal mean, but define an ASL depth and location for every year over the period 1979-2014. This results in a timeseries of 36 (1 per year for 1979-2014) SLP values for the ASL, with varying depth and location.

In this study, extreme ASL seasons are defined as the seasons from which the depth falls outside 1 standard deviation of the mean seasonal depth. Since the depth of the ASL follows a Gaussian distribution pattern, on average 32% of the values fall outside this range and are considered as extreme. For a timeseries of 36 years, this means that 6 seasons can be considered as extreme strong and 6 as extreme weak ASL seasons.

The most commonly used definition for the SAM is the normalized zonal mean pressure difference between 65° S and 40° S ($P^*_{65} - P^*_{40}$) (Gong and Wang, 1999). Based on this definition, we compute a SAM-index for every season respectively over the period 1979-2014, resulting in four timeseries of 36 index values each. For quantification of the SAM, often a distinction between higher-than-normal (positive phase) and lower-than-normal (negative phase) difference in surface pressure between high (65° S) and mid (40° S) latitudes are made[3].

The Oceanic Niño Index (ONI) from the National Oceanic and Atmospheric administration (NOAA) is a measure to record the occurrence and duration of El Niño/La Niña episodes (Glantz and Ramirez, 2020). Values for this index are 3-month running mean SST anomalies averaged over the Niño 3.4 region (5°N-5°S, 190°-240°E), compared to a centered 30 year base period. From these SST anomalies, we define an El Niño event as a period of at least 5 consecutive overlapping seasons, where the anomaly exceeds +0.5°C, likewise a La Niña event is defined with a threshold of -0.5°C. The NOAA observational data is used for the ERA5 analysis. For CESM2, we calculated the ONI ourselves in the same way, based on model SST outcome.

To investigate the combined effect of SAM and ENSO on the ASL, we created a seasonal timeseries for the entire SH with all the SLP anomalies compared to their seasonal means. Subsequently, we isolated all the seasons in which either an El Niño or a La Niña occurred. Finally, we subdivided these El Niño and La Niña timeseries further into SAM+ and SAM- timeseries. This resulted in four different combinations of El Niño/La Niña with SAM+/SAM-.

2.5 Analysis of the future climate

In order to compare the influence of the ASL on sea ice, temperature and precipitation on Antarctica for the current climate (1979-2014) with the future (2015-2100), we chose to analyse a period of equal length (2065-2100). Since we are using the extreme SSP5-8.5 scenario, this creates severely warming trends over Antarctica and surrounding areas, together with deepening trends for the ASL. We note that extreme strong ASL seasons often take place more towards the end of the period examined (2065-2100) than extreme weak ASL seasons. In order to adjust for these differences, we removed the trend in sea ice, temperature and precipitation between the average year of extreme strong and the average year of extreme weak ASL seasons. For instance, during winter the average of 6 strong ASL years is in 2088, while the average of 6 weak ASL years is in 2081. Therefore we remove a 7 year trend in sea ice, precipitation and temperature to account for this difference.

[3]Henceforth, we will refer to phases as SAM+ (SAM-) when this larger (smaller) than average difference is implied.

3 Climatology of the ASL

3.1 Surface pressure

To get a complete picture of ASL characteristics, we examine SLP values in the Amundsen-Bellingshausen and Ross Seas on a daily, monthly and seasonal timescale using the ERA5-reanalysis dataset. Figure 3 shows two examples for the daily means of the ERA5 SLP values around the AIS, for (a): summer and (b): winter. The Figure shows that on a daily basis, multiple low pressure systems move around the AIS, especially in the ASL region. Figure 2 already showed that on a yearly timescale, the ASL covers a larger spatial extent than the other two climatological lows, as well as showing the highest variability in SLP. Figure 3 suggests that this is no different on a daily basis, which makes it difficult to pinpoint the exact location of the ASL on such a short timescale. The low pressure systems around the AIS are significantly deeper on a daily timescale (Figure 3) compared to the yearly mean (Figure 2). While the ASL exhibits a yearly mean depth around 980 hPa, we observe multiple low pressure systems on a daily timescale with values around 960 hPa. As the ASL appears to represent a large cluster of smaller low pressure systems in the Amundsen-Bellingshausen and Ross Seas, we analyse the monthly and seasonal mean fields to acquire a better understanding of its climatological characteristics.

Throughout the year, the ASL features large changes in both depth (Figure 4a) and location (Figure 4b). The depth of the ASL exhibits a semi-annual pattern, with minima in April and October, and maxima during January and June. Figure 4a shows that the monthly mean surface pressure of the ASL is lowest during October (974 hPa) and highest in January (984 hPa). Green shading in Figure 4a represents the standard deviation in surface pressure per month, which has the lowest value during summer (∼4 hPa) and the highest value during winter (∼7 hPa). The zonal and meridional locations of the ASL show a similar annual cycle (Figure 4b). The ASL undergoes a meridional shift of approximately 8 degrees southward between summer and winter (-66° to -74° S). At the same time a zonal migration of 60 degrees westward is visible (270° to 210° E). These south and westward migrations seem to be much in phase and could be linked to the topography of Antarctica, as we will discuss in the next paragraph.

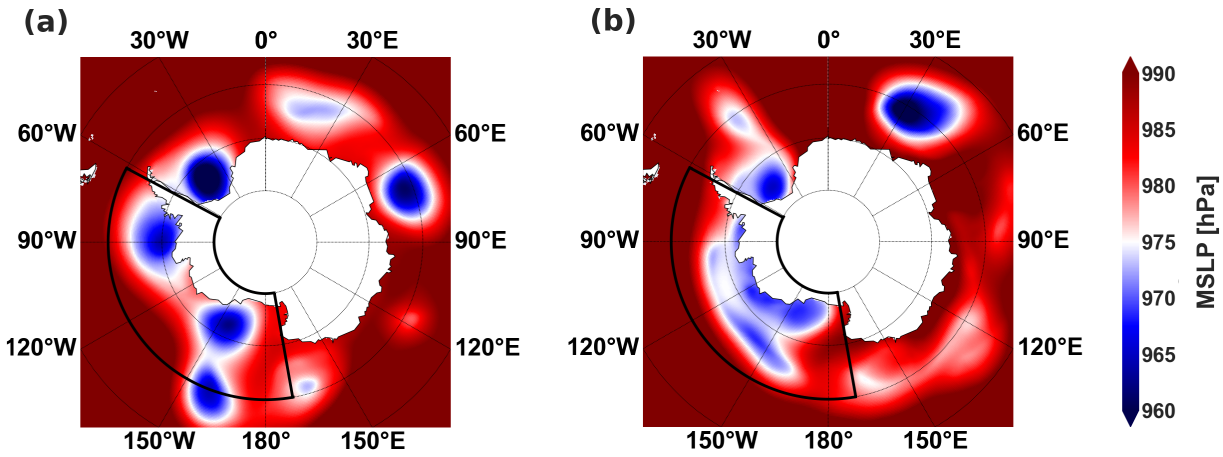

Figure 3: Two examples for both summer (a) and winter (b) show that the ASL is hard to capture on a daily timescale. The Amundsen Sea Low (ASL) is defined in the black box, bounded by 60°-80° S & 170°-298° E. ERA5-reanalysis hourly data for (a): daily mean of January 22th 1979 and (b): daily mean of June 19th 1990

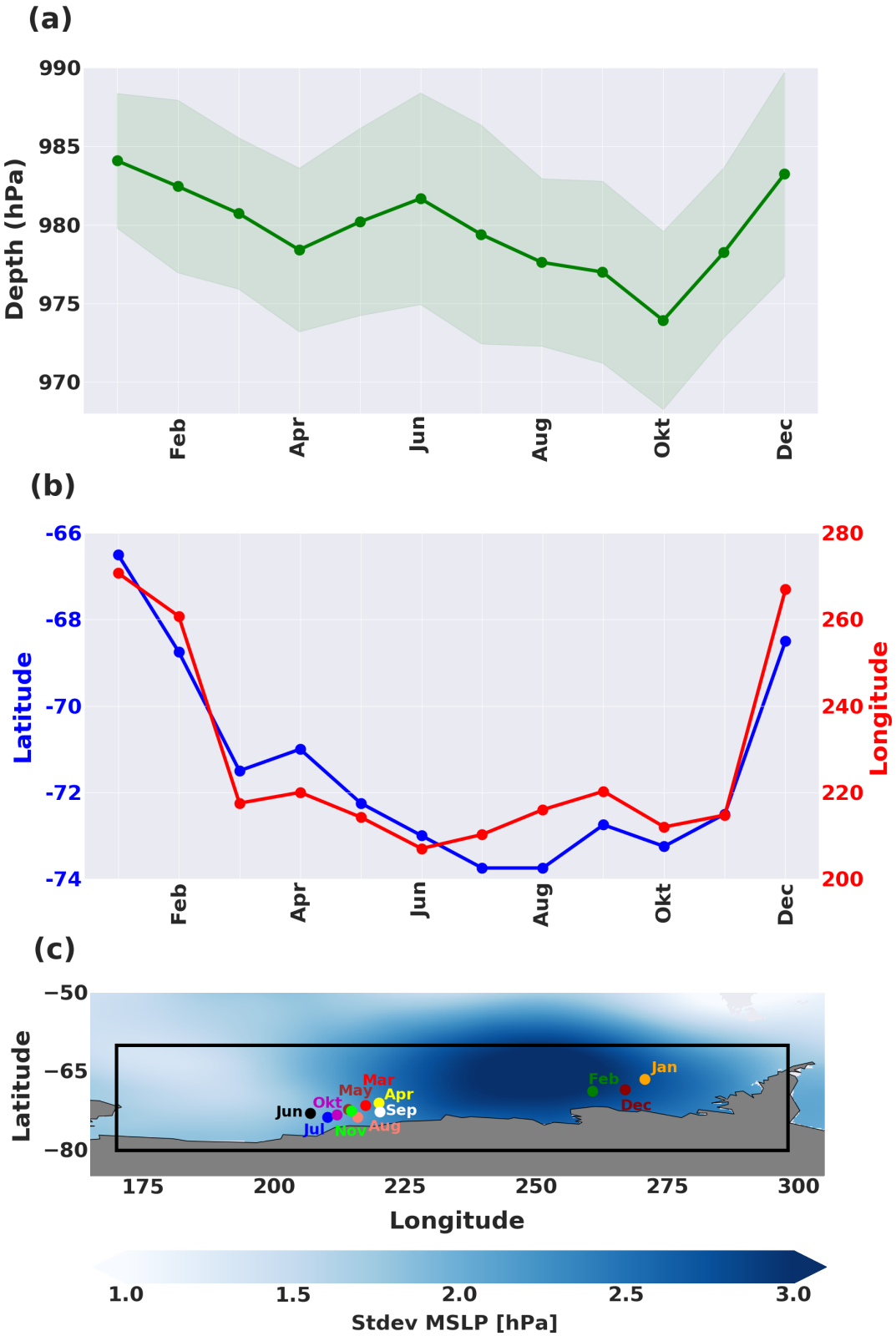

Figure 4: (a): Green line shows the ASL depth (hPa) per month, green shading represents the standard deviation in SLP per month. (b): latitudinal (blue) and longitudinal (red) position of the monthly mean ASL. (c): map of the monthly mean position of the ASL. The black box, bounded by 60°-80° S & 170°-298° E, shows the area in which the ASL is defined. The colored dots represent the monthly mean locations of the ASL, corresponding to the latitudes and longitudes from (b). The background blue shading shows the yearly standard deviation for MSLP. Data from ERA5-reanalysis, 1979-2014.

Figure 4c shows a map of the ASL region, with the colored dots representing the different monthly mean locations. Variability in MSLP (shown by the background blue shading) is largest in between the two clusters of monthly mean locations. From this map, it becomes visible that a larger cluster of points is located on the western side, which could be visualized as the median position of the ASL. The ASL is located in its median position (around 73° S, 210° E) during every season except summer. The AIS stretches further northwards on the eastern side, pushing the ASL (during summer) further north as well. The eastward migration from its median position between spring and summer will be further examined in Section 3.2, when we analyse the geopotential height field.

The ASL shows very distinctive seasonal behaviour, with the lowest surface pressure during spring and the highest in summer. There is a clear seasonality in zonal position as well, where the ASL is located around 60° more towards the east in summer compared to the other seasons. Because these ASL characteristics can be captured very well on a 3-monthly basis, we will examine ASL behaviour from now onwards on a seasonal timescale.

According to several studies (England et al., 2016; Turner et al., 2013; Goyal et al., 2021b), the ASL has undergone significant trends in both depth and location over the last several decades. Especially a deepening during austral summer has been observed, linked to the loss of stratospheric ozone. We calculated these monthly, seasonal and yearly trends as well, over the period 1979-2014. Significance was checked using a two-tailed Student's t-test, assuming a Gaussian distribution. Our results show that for monthly, seasonal and yearly timeseries, no significant ASL trends can be found at the 95% confidence level, although we do find MSLP deepening in parts of the ASL region, especially during austral summer and autumn (Figure 5). The Figure also shows that for all seasons, no significant trends are found in the ASL region. The question arises why previous studies found trends in the ASL whereas we do not. Our current interpretation is that this is caused by the relatively short observational period combined with the ASL's high variability, which makes it hard to calculate robust statistics. Trends found in other studies depend much on the chosen time period and we found them therefore to be insignificant.

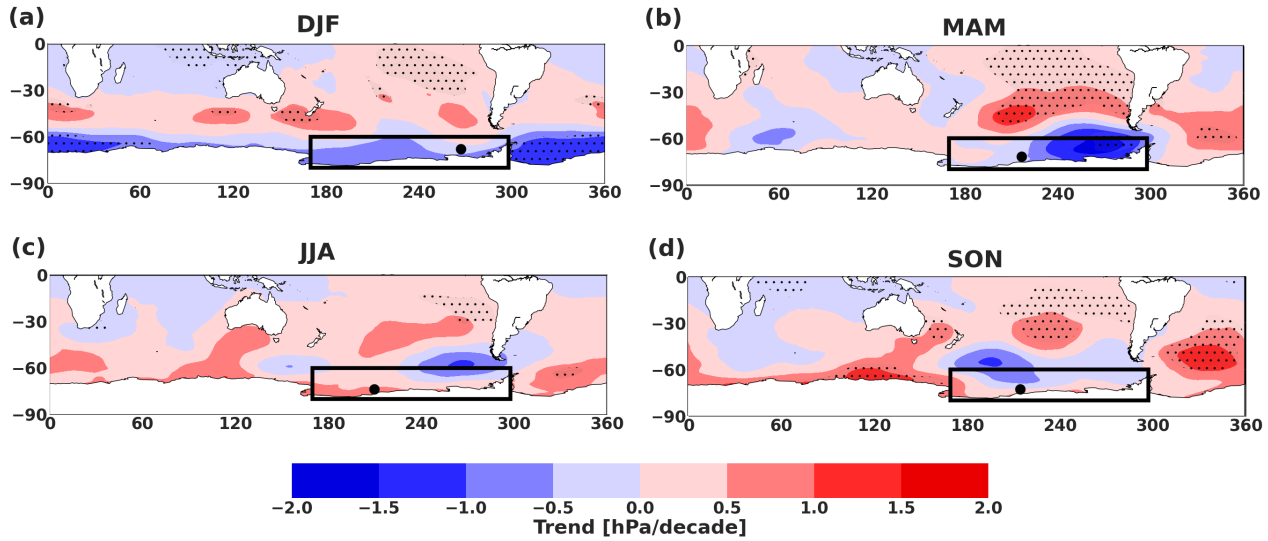

Figure 5: Trend in SLP on the SH in units of hPa/decade for (a): summer, (b): autumn, (c): winter and (d): spring. The ASL is defined in the black box, bounded by 60°-80° S and 170°-298° E. The larger black dots represent the seasonal mean position of the ASL. The smaller black dots indicate where correlations are significant at the 95% confidence level. Data from ERA5-reanalysis, 1979-2014.

3.2 Geopotential height

From the previous section, the question arises why the ASL summer position differs from the other seasons. To explain this, we analyse the 500hPa geopotential height field (Z500). A surface low pressure system is commonly linked to a trough in the higher troposphere, where the upper level trough is often located slightly more to the east (Turner et al., 2013). From examining the Z750, Z500 and Z250 fields, we find that the ASL, as well as the other two climatological low pressures systems, are found throughout the depth of the troposphere (not shown). Figure 6 shows the seasonal mean Z500 field, with the surface location of the ASL represented by the black and white dots. For every season, the upper level trough exists at roughly the same location, above the Ross Ice Shelf. However, we do observe a significant 150-250 m difference in depth of the upper level trough between austral summer and the other seasons. This causes the Z500 meridional flow component around the trough to be weaker in summer, allowing a further eastward migration of the surface lows in this season.

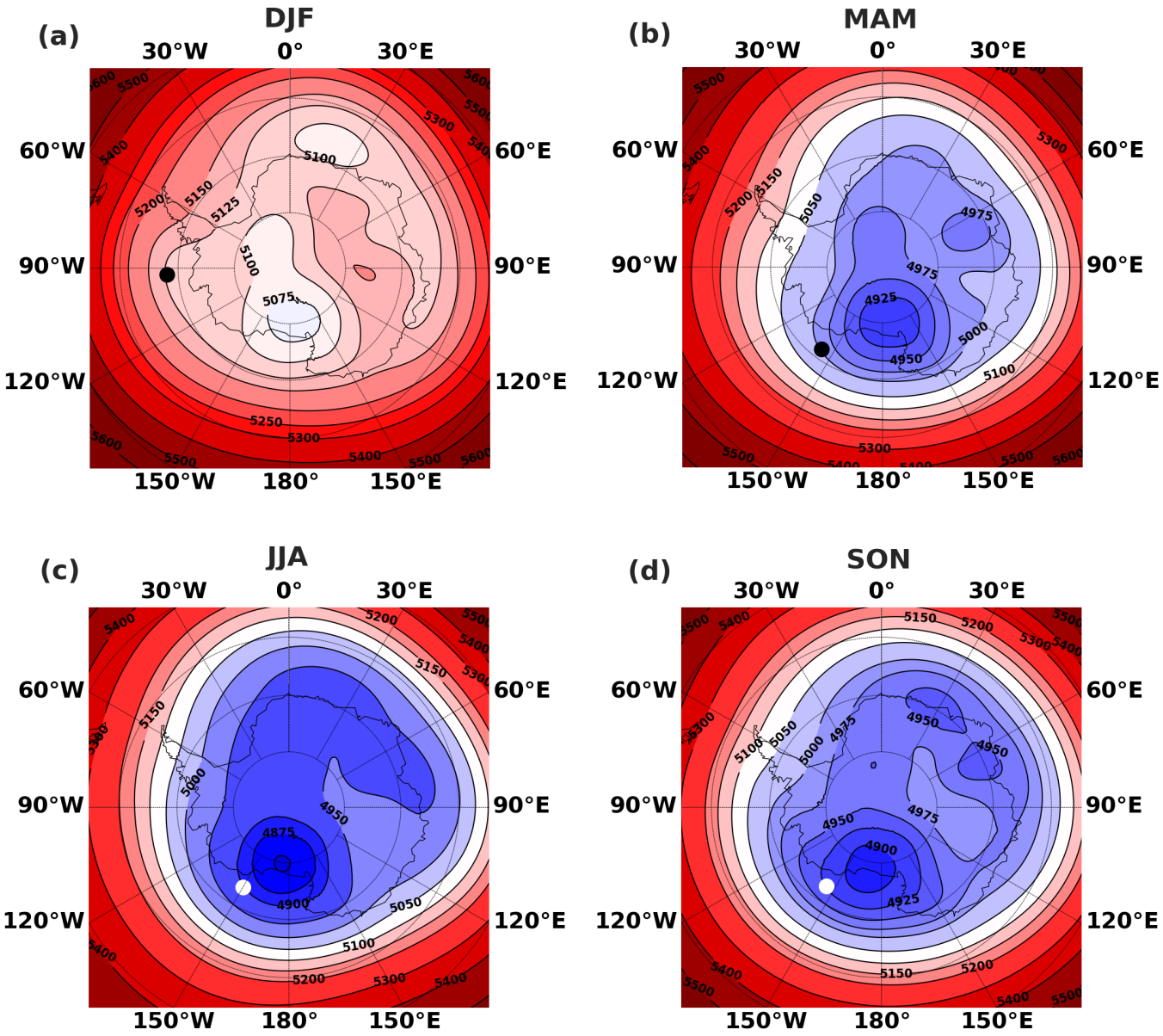

Figure 6: Z500 geopotential height field for (a): summer, (b): autumn, (c): winter and (d): spring. The black/white dots mark the position of the seasonal mean ASL. Contour lines are displayed in meters, with varying intervals. Data from ERA5-reanalysis, 1979-2014.

3.3 Evaluation of CESM2

So far, we have described the ASL using the ERA5-reanalysis data. Next, we are interested how the ASL is represented in the free-running climate model CESM2. For the purpose of model evaluation, we compare CESM2 to ERA5 for the seasonal SLP fields at high SH latitudes. The result shows that CESM2 underestimates the depth of the SLP field in the Southern Ocean by ∼5-10 hPa. However, the large scale patterns in SLP simulated by CESM2, show a high degree of similarity to ERA5. The results for the seasonal SLP analysis are shown in Figure 7 (left: ERA5, right: CESM2). In order to show these similar large scale patterns, taking into account the underestimated SLP values by CESM2, we chose two different scale bars (ERA5: 975-990 hPa, CESM2: 965-990 hPa).

CESM2 captures the seasonality in ACT strength relatively well, which is weakest during summer and deepest during spring. Both zonal location and spatial extent of the three climatological lows show very similar patterns between model and observations. The relative strength of the ASL compared to the complete Southern Ocean SLP field is best simulated during summer (DJF) and spring (SON). During autumn (MAM) and winter (JJA), CESM2 overestimates the depth of the ASL compared to the other two climatological low pressures systems. RMSLP patterns are analysed as well (not shown) because they hold a strong importance in driving surface winds and therefore influences temperature, precipitation and SIE over Antarctica (Hosking et al., 2013). We find that the zonal MSLP is often underestimated by CESM2 in the same way as the absolute MSLP field, causing RMSLP patterns to be very similar to ERA5. The largest model biases arise from comparing the central location of the ASL (represented by the dots in the black box) between ERA5 and CESM2. With the results from ERA5, we showed before that the ASL is positioned close to the AP during summer and in its median position near the Ross Sea during the other seasons. CESM2 simulates the ASL location to be more centered in between those two locations, with largest differences to ERA5 observed in winter and spring.

Although these (relatively small) model biases cause some differences in simulating the influence of the ASL on Antarctica, we deem CESM2 to be representative enough for further use. In the next section, we will further examine ERA5 and CESM2 on the topic of tropical teleconnections.

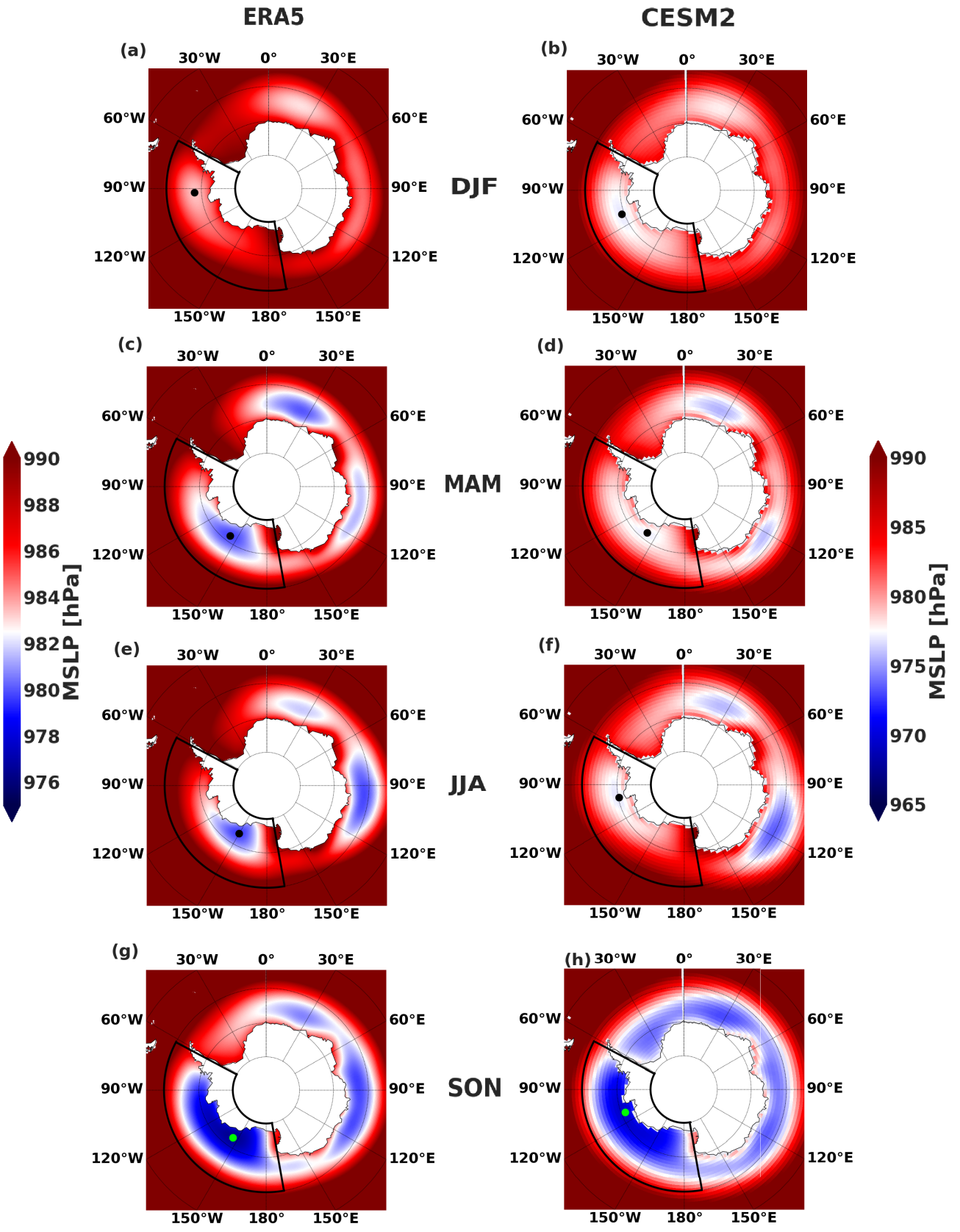

Figure 7: Seasonal SLP where we compare ERA5 data (left; a,c,e,g) with CESM2 (right; b,d,f,h). The ASL is defined in the black box, bounded by 60°-80° S and 170°-298° E. The dots in the black box represent the seasonal mean locations of the ASL for DJF (a,b); MAM (c,d); JJA (e,f); SON (g,h). Note the different scale bars on the left (ERA5) and the right (CESM2). Data for the period 1979-2014.

4 Links with large scale oscillations

4.1 SAM

The depth of the ASL is strongly influenced by the Southern Annular Mode, which is the leading mode of atmospheric variability in the SH (Marshall, 2003). The SAM is represented as an asymmetric seesaw in surface pressure between mid (40° S) and high (65° S) latitudes. As a rule of thumb, total hemispheric mass conservation suggests that a negative pressure anomaly for the Antarctic region must be balanced by a positive anomaly equatorward (Visbeck, 2009). The asymmetry results from the exchange of mass between larger (mid-latitudes) and smaller areas (high-latitudes). This often results in highest pressure anomalies observed at the highest latitudes, because the area over which atmospheric mass gets redistributed is smaller.

Table 1 lists the seasonal correlation coefficients and the regression slopes between the ASL-index and the SAM-index for ERA5 and CESM2. The result shows that the ASL and SAM are strongly negatively correlated for all seasons. This can be interpreted as a SAM+ season holding a strong relation with a negative ASL pressure anomaly, and vice versa. Coefficient values are in between -0.75 and -0.89 (all significant at the 95 % confidence level), which CESM2 also simulates remarkably well. The regression slopes show slightly larger discrepancies, however, the order of magnitude (around 1) is similar for every season (i.e., a 1 hPa anomaly for the SAM results in a 1 hPa anomaly for the ASL).

Besides calculating regression slopes between the SAM-index and ASL-index, we regress the 1D SAM-index to the 3D SLP field to reveal the impact of the SAM on the surface pressures of the entire SH. The result shows that the influence of SAM variability is not restricted to the ASL region but affects pressure on the entire extratropical SH (Figure 8). The asymmetric seesaw pattern is illustrated with larger negative anomalies at high-latitudes countered by smaller positive anomalies at mid-latitudes. We note that differences in ASL location between ERA5 and CESM2 have no significant impact on correlations with the SAM (which is shown as well by the large similarities in Table 1), since these are strongly negative and significant for the entire SH high-latitudes.

For both summer and winter, the spatial regression patterns in Figure 8, show large similarities between ERA5 and CESM2. Comparable to the results of Table 1, seasonal differences in impact of the SAM on the SLP field are small. Pressure anomalies in the ASL region as a response to anomalies in the SAM vary between ∼-0.75 and ∼-1.25 hPa for all seasons. A notable seasonal difference in Figure 8 is that the area of significant correlations at mid-latitudes covers a much larger spatial extent during summer (DJF) than during winter (JJA). Even this relatively small seasonal contrast is captured with a high degree of resemblance by CESM2.

Table 1: Seasonal correlation coefficients and regression slopes between the ASL-index and the SAM-index for ERA5 and CESM2 (1979-2014). All numbers are significant at the 95% confidence level.

	Correlation		**Regression Slope**	
	ERA5	**CESM2**	**ERA5**	**CESM2**
DJF	-0.79	-0.81	-0.85	-1.31
MAM	-0.81	-0.75	-1.02	-0.85
JJA	-0.84	-0.81	-1.08	-0.73
SON	-0.81	-0.89	-0.99	-1.18

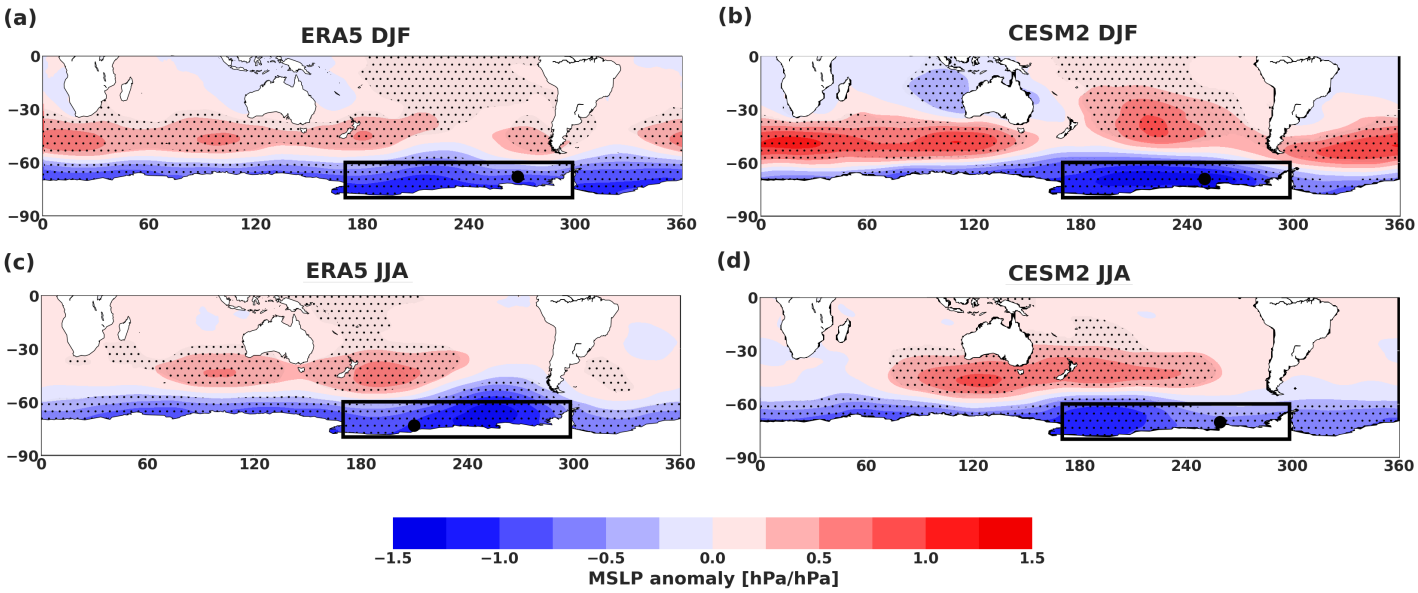

Figure 8: Regression of SLP against the SAM-index. Positive (negative) values correspond to positive (negative) SLP anomalies per hPa increase in the SAM (i.e., per hPa increase in $(P^*_{65} - P^*_{40})$). In the columns we vary the model, in the rows we vary the season. The ASL is defined in the black box, bounded by 60°-80° S ad 170°-298° E. The larger black dots represent the seasonal mean position of the ASL. The smaller black dots indicate where correlations are significant at the 95% confidence level. Data from ERA5 and CESM2, 1979-2014.

The opposing pressure anomalies between the mid and high latitudes of the SH implies that the SAM fundamentally represents changes in the meridional pressure gradient across the SH and the corresponding meridional location and intensity changes in the polar jet stream encircling Antarctica (Fogt and Marshall, 2020). As such, SAM variability and the associated trends, shown by the timeseries in Figure 9a, represent changes in the extratropical atmospheric circulation. The figure shows seasonal timeseries for the SAM-index (a) and the ASL-index (b) for both ERA5 and CESM2.

We observe strong negative correlations between the timeseries in Figure 9a and 9b, which is to be expected from the results of Table 1 and Figure 8. For instance, comparing the two CESM2 timeseries we observe two large downward peaks from the SAM-index in 1989 and 1994, corresponding with two large upward peaks in the the ASL-index during the same years. Furthermore, we observe two large upward peaks from the ERA5 timeseries in Figure 9a in 1999 and 2011, corresponding with two downward peaks in Figure 9b during the same years. The standardized SAM-index shows trends towards more positive values for both the ERA5 and CESM2 timeseries. Subsequently, the ASL follows a deepening trend according to both the model and observations. Both the amount of variability (shown by the values for stdev) as well as the direction of the trendlines show large resemblances, although CESM2 overestimates the slopes of the long term trends.

There is consensus in previous studies (Marshall, 2003; Visbeck, 2009; Fogt and Marshall, 2020) that the SAM shows a trend towards more positive values over the last several decades. This positive trend agrees with our results from the timeserie analysis. However, this significant positive trend does not exist in our results for every season, as they show large seasonal differences. Both ERA5 and CESM2 are in agreement that significant ($p < 0.10$) positive SAM trends since 1979 are only observed in austral summer and autumn, although the values of the slopes differ slightly between model and observations. During winter and spring, no significant

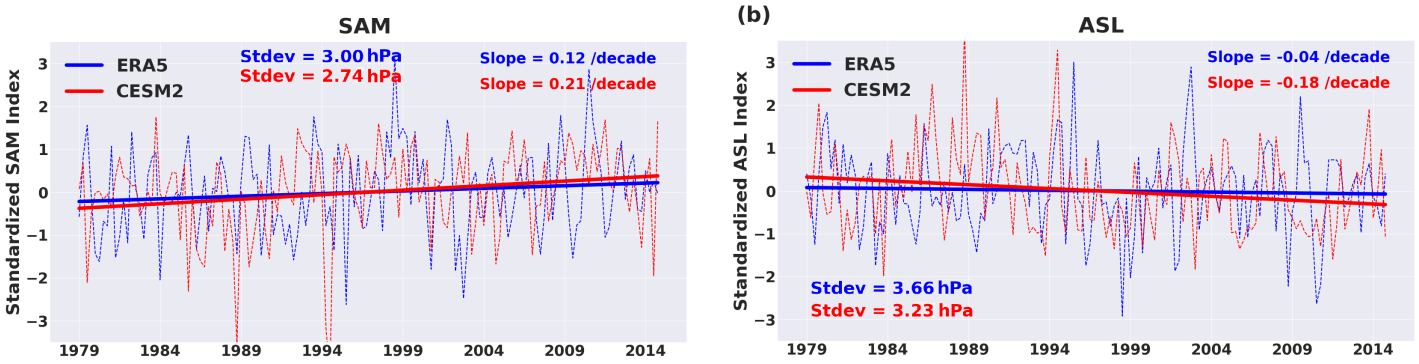

Figure 9: Seasonal timeseries and associated trends for (a): the SAM and (b): the ASL, in which every time-step represents an anomaly as a function of its own seasonal mean. The dashed lines show the seasonal variations and the solid lines represent the trends. The timeseries are standardized, which means that its variability is measured in units of its own standard deviation (shown on the y-axis). The stdev values in units of hPa are given as well. The calculated slopes in units: stdev/decade are shown at the top right corner. Data from ERA5 (blue) and CESM2 (red), 1979-2014.

SAM trends are observed. The positive SAM trends during summer and to a lesser extent during autumn are often linked with the loss of stratospheric ozone (Goyal et al., 2021c; Fogt and Marshall, 2020; Visbeck, 2009). Although the ozone hole is a feature of austral spring, the strongest changes in atmospheric circulation are often seen during the subsequent season (i.e., summer).

The ASL does not show any significant ($p < 0.10$) trends on a seasonal timescale over the last decades, which is not expected based on its strong negative relation with the SAM that does show significant trends. The observed seasonal ASL trends are predominantly (both ERA5 and CESM2) positive, for which the insignificance is probably caused by its large natural variability. Our results show a larger disagreement between ERA5 and CESM2 for the ASL trends than for the SAM trends. Possible explanations for this are the differences in modelled ASL location (Figure 7) and the 20% (shown by the values for stdev in Figure 9) larger natural variability of the ASL, which tends to obscure trends in this relatively brief (36 years) timeseries.

4.2 ENSO

Table 2: Seasonal correlation coefficients and regression slopes between the ASL-index and the ENSO-index for ERA5 and CESM2 (1979-2014). Bold numbers are significant at the 95% confidence level.

	Correlation		**Regression Slope**	
	ERA5	**CESM2**	**ERA5**	**CESM2**
DJF	**0.50**	**0.61**	**1.65**	**1.33**
MAM	0.10	0.16	0.43	0.26
JJA	0.32	0.00	2.16	0.39
SON	0.23	**0.38**	1.07	**1.06**

Another important driver of the ASL is ENSO (Scott Yiu and Maycock, 2019; Clem et al., 2017; Turner et al., 2013). The response of the ASL region to ENSO variability can partly be explained by its location in the Southern Pacific, where Rossby waves from the tropics associated with ENSO variability have a year-round effect (Goyal et al., 2021a; Raphael et al., 2016). ENSO undergoes a strong seasonal cycle (Timmermann et al., 2018), with largest SST and wind anomalies occurring during austral summer.

Table 2 lists the seasonal correlation coefficients and the regression slopes between the ASL-index and the ENSO-index for ERA5 and CESM2. The largest and most significant correlations occur during austral summer, which is expected since ENSO-events often peak around December. The other seasons demonstrate weaker correlations which are mostly insignificant. Similar to the results obtained from the SAM analysis (Table 1), the correlations show a high level of agreement between CESM2 and ERA5. It is a positive result for CESM2 (in which no observations are assimilated) that it is able to simulate the seasonality of this tropical teleconnection. ENSO and the ASL show positive correlations throughout the year, which can be interpreted as a positive SST anomaly in the Niño 3.4 region that is linked with a positive SLP anomaly for the ASL and vice versa. The relative magnitude of the regression slopes listed in Table (2) is mostly in line with the relative magnitude of the correlation coefficients (i.e., a larger seasonal correlation correspond with a larger seasonal regression slope). Slopes larger than 1 hPa/degree for both ERA5 and CESM2 are observed during austral spring and summer, which are the seasons with the largest SST anomalies in the Niño 3.4 region as well. ERA5 and CESM2 feature rather similar values for the regression slopes, except during winter. This large model bias in winter can be linked to the large difference in ASL location during that season (Figure 7), which will be further examined in the next paragraphs.

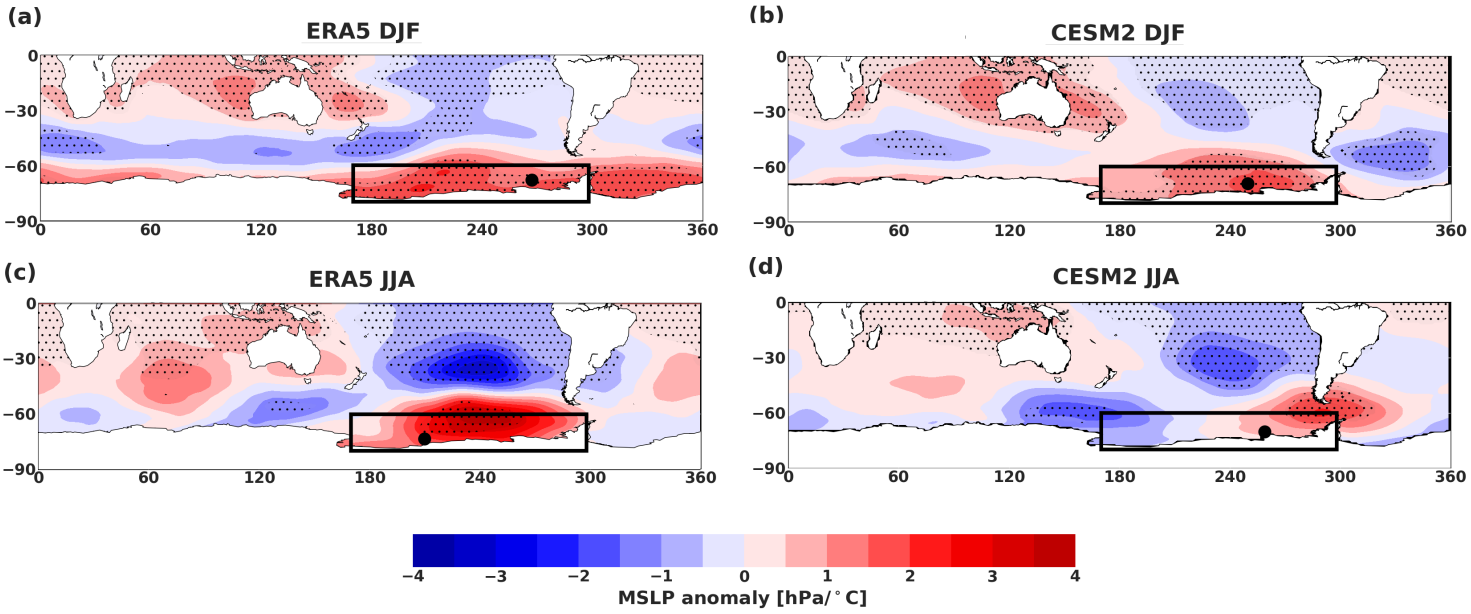

Figure 10: SLP anomalies for the SH as a response to anomalies in the ENSO-index. Positive (negative) values correspond to positive (negative) SLP anomalies per degree (SST) increase in the Niño 3.4 region. In the columns we vary the model, in the rows we vary the season. The ASL is defined in the black box, bounded by 60°-80° S and 170°-298° E. The larger black dots represent the seasonal mean position of the ASL. The smaller black dots indicate where correlations are significant at the 95% confidence level. Data from ERA5 and CESM2, 1979-2014.

Figure 10 shows the result of the regression analysis between the 1D ENSO-index and the 3D SLP-field in the SH for both summer (a,b) and winter (c,d). Predominantly positive SLP anomalies are visible in the ASL region for all seasons, which is expected from the positive correlations listed in Table 2. These positive correlations can be interpreted as follows: during the El Niño (La Niña) phase, a positive (negative) temperature anomaly is observed in the tropics, which will cause positive (negative) SLP anomalies in the Amundsen-Bellingshausen and Ross Seas and thus weaken (strengthen) the ASL. This is consistent with results found in the literature. Pope et al. (2017) states that during the El Niño phase, a Rossby wave train of alternating positive and negative geopotential height anomalies extends from the tropics to the ASL region, often described as the positive polarity of the Pacific-South American teleconnection pattern. This is associated with a weakening of the ASL. Subsequently, Coggins and McDonald (2015); Raphael et al. (2016) find a deepening of the ASL during the La Niña phase.

Another interesting result from Figure 10 are the seasonal differences. Although ENSO-events generally peak in austral summer, the weakest SLP anomalies in the ASL region occur during that season. However, Figure 10 shows that the spatial extent of significant positive correlations on high-latitudes is largest during summer for both ERA5 and CESM2. This causes the location of the ASL to be an unimportant factor in obtaining high correlation values for the summer season. During winter we observe larger SLP anomalies in the ASL region, however, these large anomalies cover a much smaller spatial extent. We note that for both ERA5 and CESM2 the location of the ASL falls just outside the area of large SLP anomalies and significant correlation values during winter, which explains the small correlations found in Table 2. For both spring and autumn (not shown), patterns are similar as for winter, with large anomalies up to 4 hPa/°C in the ASL region. However, these large SLP anomalies are often found more towards the east than the mean location of the ASL. During all seasons except summer, the location of the ASL is an important factor in the calculated correlations and slopes between the ASL-index and the ENSO-index. As a result, the calculated values listed in Table 2 do not provide a clear picture of the SLP anomalies observed in the ASL region and these numbers are therefore not completely robust.

4.3 Combined co-variance of the ASL with SAM and ENSO

As a final step in investigating the relationship between the two large modes of climate variability and the ASL, we examine the combined effect of SAM and ENSO. The resulting SLP anomalies as a consequence of the four different combinations of El Niño/La Niña with SAM+/SAM- are shown in Figure 11. Comparing the combinations involving SAM+ seasons (a,b,e,f), we note predominantly negative anomalies at high latitudes and positive anomalies at mid latitudes. For combinations including SAM-, this pattern is reversed. These patterns suggest that the SAM is a more important modulator of surface pressure at the mid and high latitudes. Comparing combinations including either El Niño (a,b,c,d) or La Nina (e,f,g,h), we note large similarities at low latitudes and in the Pacific Ocean. This suggests that ENSO is a more important modulator of surface pressure at low latitudes as well as having large influences on SLP in the entire Pacific Ocean. Since the SAM influences SLP at mid and high latitudes and ENSO has an effect on surface pressures in the entire Pacific section, these two effects are combined in the Southern Pacific Ocean, which is the region of the ASL.

From Figure 11, we note that the combination of either El Niño with the negative SAM polarity (c,d) or La Niña with the positive SAM polarity (e,f), strengthens pressure anomalies in the ASL region significantly. We observe strong positive SLP anomalies in the Southern

Pacific when El Niño occurs with SAM- (c,d), resulting in an anomalous weak ASL. When La Niña occurs with the positive SAM polarity (e,f), large negative anomalies are observed, resulting in an anomalous strong ASL. Other ENSO/SAM combinations (a,b,g,h) do not have a large impact on the ASL region, since only small pressure anomalies are found

The large scale patterns in SLP as well as amplification/reduction of pressure anomalies in the ASL region are well represented in CESM2. Both combinations El Niño and SAM- (c,d), and La Niña and SAM+ (e,f) show similar pressure anomalies for CESM2 and ERA5. However, we note that these large surface pressure anomalies are predominantly concentrated in the eastern part of the ASL region, which causes the difference in ASL location between ERA5 and CESM2 to be an important factor in the observed strengthening/weakening of the ASL. Figure 11 shows that the mean ASL location is found more towards the east in CESM2 compared to ERA5, which results in differences in strengthening/weakening of the ASL. For instance, comparing sub-figure c and d, CESM2 shows a SLP anomaly of 6 hPa for the ASL, while ERA5 only shows an anomaly of 3 hPa. While similar large scale patterns are observed between ERA5 and CESM2, the difference in ASL location causes some model biases.

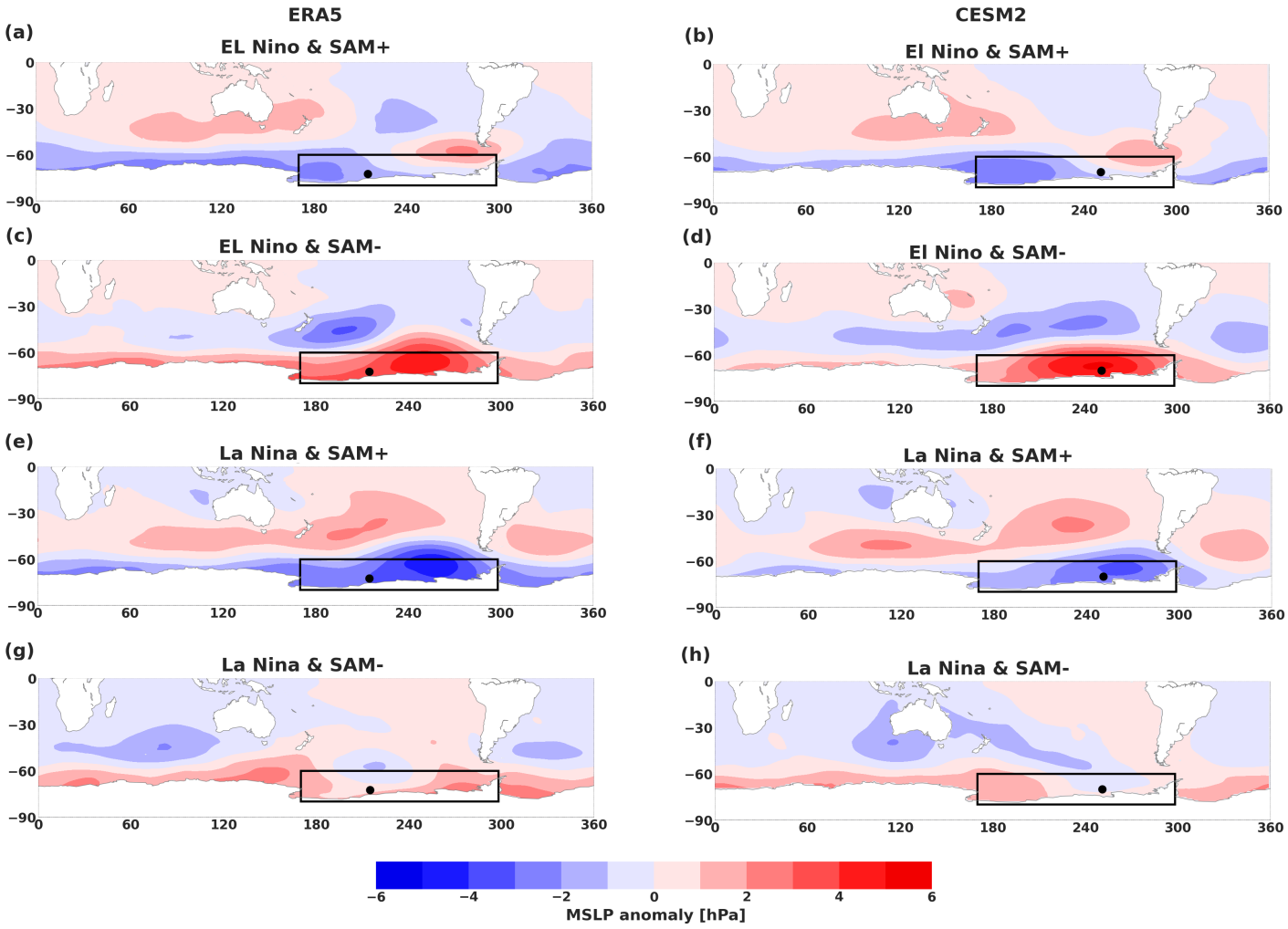

Figure 11: Seasonal SLP anomalies in the SH calculated with the combined effects of SAM and ENSO. El Niño (La Niña) indicates seasons where the SST in the Niño 3.4 region is larger than (smaller than) 0.5° compared to the seasonal mean. Further subdivision into SAM+ (SAM-) is based on the SAM-index being larger (smaller) than its seasonal mean. In the columns we vary the model, in the rows we vary the different SAM/ENSO combinations. Data from ERA5 and CESM2, 1979-2014.

5 Influence on the Antarctic climate

The ASL has shown to be an important regulator of West Antarctic climate, controlling surface winds in the Ross, Amundsen and Bellingshausen Seas (Coggins and McDonald, 2015; Turner et al., 2016; Raphael et al., 2016). Hosking et al. (2013) showed that the impact of the ASL on the West Antarctic Ice Sheet is directly related to ASL variability in zonal location and depth, creating both positive and negative anomalies in temperature and precipitation over West Antarctica. In this section we examine the impact of extreme (strong and weak) ASL seasons on the sea ice budget in the Southern Ocean, especially focusing on the Ross, Amundsen and Bellingshausen Seas. Furthermore temperature and precipitation anomalies across Antarctica and its ice sheet are analysed.

5.1 Sea ice extent

Sea ice extent (SIE) represents the area for which the fraction of sea ice is at least 15%. Sea ice concentration (SIC), indicates the fraction of sea ice for individual grid cells. Figure 12 shows anomalies in SIC for the difference between strong (+ 1σ) and weak (- 1σ) ASL years for summer (a,b) and winter (c,d). The difference in SLP between these strong and weak ASL years is shown as well over the Southern Ocean. The white area around the AIS indicates the SIE, which is larger ($\pm$3 times) during winter (c,d) than during summer (a,b). The results from ERA5 (a,c) indicate that a stronger ASL causes predominantly positive SIC patterns over the Southern Ocean during all seasons (spring and autumn are not shown). We note that during winter, the areas of positive and negative SIC anomalies are grouped into larger clusters than during summer. From Figure 4a, we already observed that the absolute depth of the ASL is lower during winter than during summer, as well as having a larger value for the stdev. From comparing Figure 12a with Figure 12c, we note that this is no different and larger SLP anomalies are observed during winter, especially over the ASL region. We calculate the average SIC anomaly associated with the strength of the ASL for every season. The largest increase (between 2 and 2.5%) occurs during winter and spring, which are the seasons where we also observe the largest variability in SLP. During summer and autumn, only small increases in SIC are observed (between 0 and 0.5%).

Variability in SIC associated with a stronger ASL consists of predominantly negative anomalies close to the AP and positive anomalies over the Ross Sea. These opposing patterns on the eastern and western side of the ASL region (which are strongest during winter) are probably related to surface wind directions around a cyclone. Surface winds around low pressure systems flow in a predominantly clockwise rotation in the SH. This is translated to the ASL region as a northerly flow towards the AP, transporting relatively warm and moist air and a southerly flow over the Ross Sea, transporting relatively cold and dry air away from Antarctica. Comparing strong with weak ASL seasons, we observe large anomalies in SLP over the Amundsen-Bellingshausen and Ross Seas and therefore an increase in strength of these surface winds over the entire ASL region. This leads to additional sea ice growth in the Ross Sea and sea ice melt close to the AP.

CESM2 (Figure 12b and d) overestimates the total SIE slightly for every season. However, the strong seasonality, in which the winter extent is three times larger than the summer extent, is well modulated. CESM2 underestimates the SLP patterns associated with a stronger ASL to some extent, where the largest differences with ERA5 are observed during winter. Subsequently, we note that the area of largest SLP anomalies during winter is concentrated over the Ross Sea, which is much further westward than any seasonal mean position of the ASL and therefore not

very realistic. During other seasons, the largest SLP patterns are observed at a similar location as from ERA5. CESM2 Calculates the average SIC anomaly similar to ERA5 with increases during most seasons except summer, when we observe a small decrease (Figure 12b).

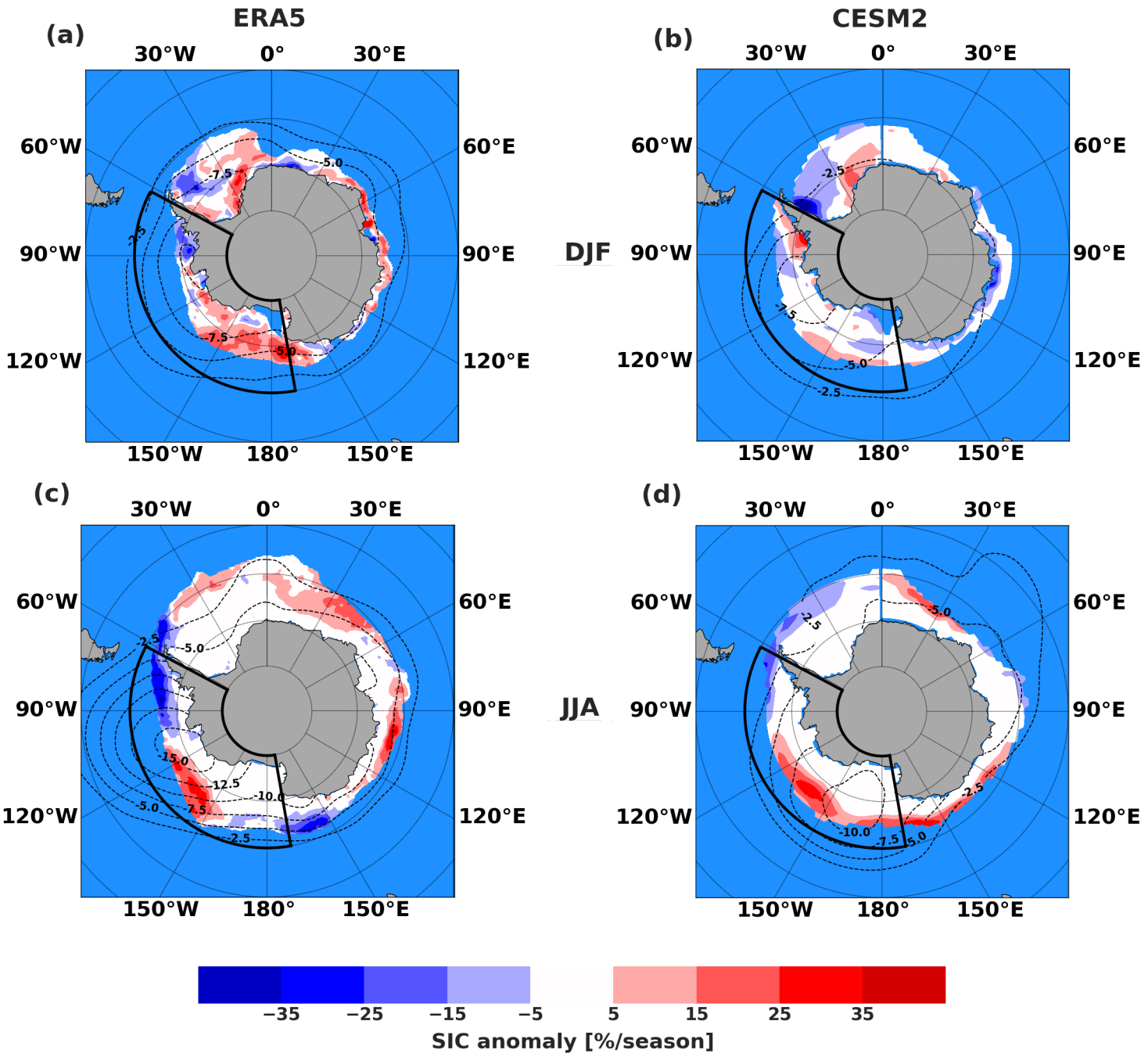

Figure 12: Sea ice concentration (SIC) anomalies around the AIS for the difference between strong (+ 1σ) and weak (- 1σ) ASL seasons. In the columns we vary the model, in the rows we vary the season. The white area around Antarctica indicates the SIE where more than 15% sea ice is present during that season. The black box shows the ASL region (60°-80° S, 170°-298° E) and the contour lines with intervals of 2.5 hPa display the anomalies in surface pressure over the Southern Ocean. Data from ERA5 and CESM2, 1979-2014.

5.2 Temperature

Figure 13 shows Temperature anomalies over Antarctica together with anomalies in SLP over the Southern Ocean, for summer (a,b) and winter (c,d). Anomalies are obtained in the same way as for SIC, by examining the difference between strong and weak ASL seasons. We observe predominantly negative temperatures over the AIS in cases where the ASL is strong, especially in East Antarctica. Furthermore, we note stronger patterns during the winter season, which was a result obtained as well from the sea ice analysis. In ERA5, the average temperature over Antarctica decreases the most significant during autumn and winter ($<$ -1°C), while smaller decreases are calculated during spring and summer ($\sim$-0.5°C). The net cooling effect over Antarctica as a result of ASL deepening, can be explained with larger scale meteorology. Since the ASL holds strong relations with the SAM, we observe strong positive SAM seasons to coincide with deep ASL seasons. Simple geostrophic balance tells us that a positive SAM results in a strong westerly wind around Antarctica, causing less meridional exchange to transport warm air from lower latitudes, thus keeping temperatures low over the AIS.

The SLP anomalies from Figure 13 show a difference in depth of up to 10 hPa during summer and 15 hPa during winter (ERA5). The strongest SLP anomalies are observed around the center of the ASL region during all seasons except summer, for which its position is more towards the east, due to its more eastern absolute location. These stronger SLP patterns during winter are probably a cause of the larger temperature anomalies observed during that season. Another explanation can be the larger horizontal and vertical temperature gradients during winter, making temperature more sensitive to advection. Although the dominant response shows negative temperatures over Antarctica, we observe positive anomalies in the ASL region as well. These positive temperature anomalies are predominantly concentrated east of the largest SLP anomalies, where the dominant meridional wind direction is northerly. During summer, we note these positive patterns solely over the AP, while in winter the area extents further along the coast, as well as over the Ronne Ice Shelf and the Transantarctic Mountains. Calculations over exclusively the ASL region show an average temperature increase of almost 1°C during winter and spring (ERA5).

The average temperature anomalies over Antarctica calculated from CESM2 are qualitatively similar to those from ERA5. CESM2 shows negative temperatures associated with a strong ASL for all seasons. During winter and spring even larger decreases ($<$-1.5°C) are observed than from ERA5. We note from Figure 13 that the larger temperature patterns show strong similarities between model and observations. However, some differences are observed as well; the large areas of positive anomalies over the ice shelfs and the Transantarctic Mountains during winter are almost completely absent in CESM2. Furthermore, we note that CESM2 underestimates the negative temperature responses over East Antarctica during all seasons. As there appears to be a link between the strength of the SLP anomalies over the Southern Ocean and the strength of the temperature anomalies over Antarctica, this agrees with the smaller patterns observed from CESM2.

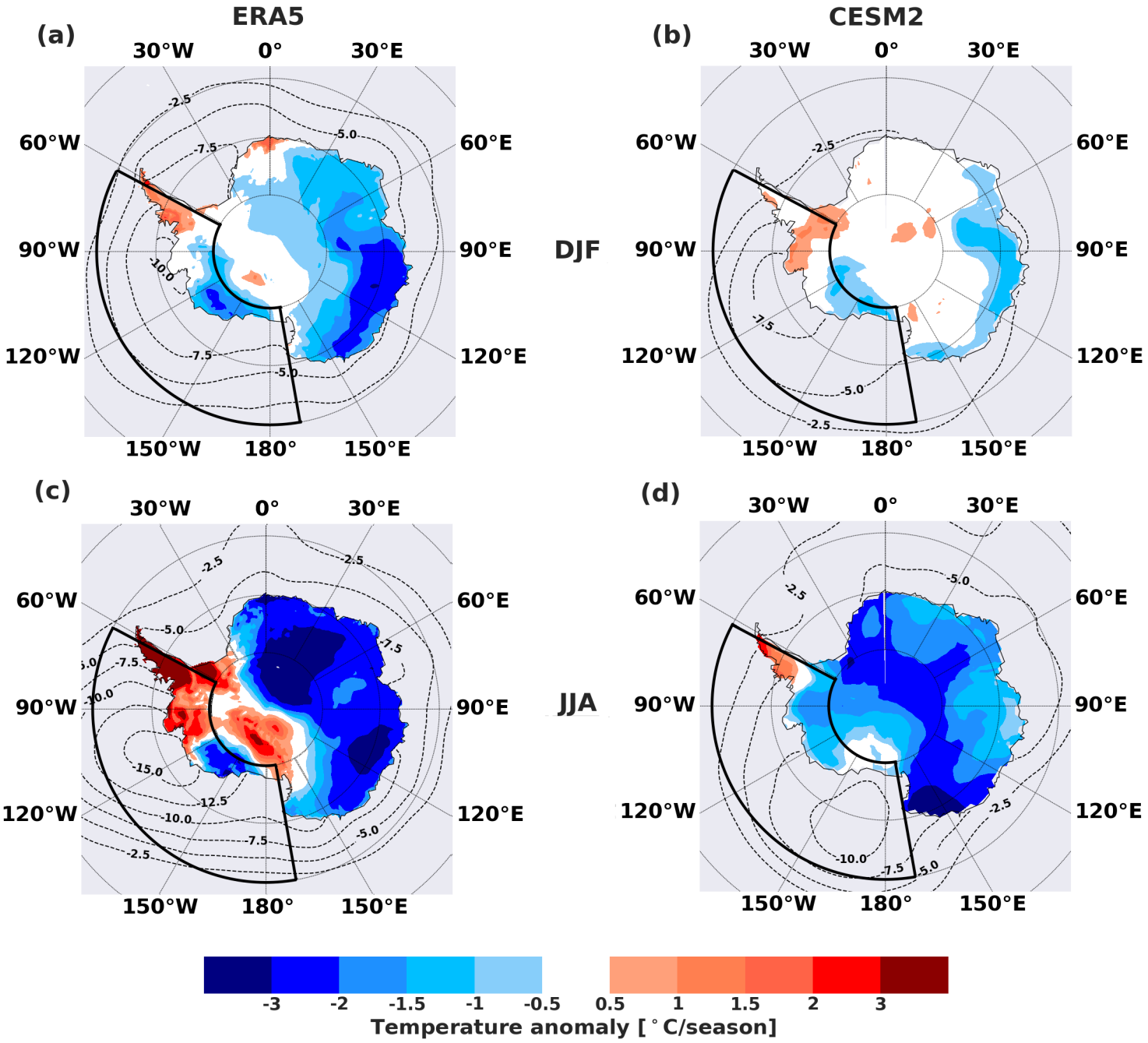

Figure 13: Temperature anomalies over Antarctica for the difference between strong (+ 1σ) and weak (- 1σ) ASL seasons. In the columns we vary the model, in the rows we vary the season. The black box shows the ASL region (60°-80° S, 170°-298° E) and the contour lines with intervals of 2.5 hPa display the anomalies in surface pressure over the Southern Ocean. Data from ERA5 and CESM2, 1979-2014.

5.3 Total precipitation

The total surface mass balance (SMB) over the AIS is largely determined by total precipitation (Lenaerts et al., 2012). On Antarctica in general, total precipitation (both solid and liquid) occurs predominantly in the form of snow and the AIS surface is usually too cold for substantial sublimation and melt to occur. For that reason, SMB and solid precipitation can be assumed as quasi-equivalent (Maclennan and Lenaerts, 2021). Total precipitation usually peaks along the coastal margins of the AIS, where the surface is steep and meridional surface winds transport relatively humid air from the Southern Ocean towards Antarctica (Van Wessem et al., 2014). Precipitation patterns over the AIS are largely determined by topography, due to the dominant contribution of orographic forcing (Lenaerts et al., 2012). However, regional patterns are influenced by meridional surface winds as well, in which the forcing of low pressure systems such as the ASL plays an important role.

Figure 14 shows the seasonal precipitation anomalies over the AIS for the difference between strong (+ 1σ) and weak (- 1σ) ASL seasons. Examining the results from ERA5 (Figure 14a and c), we note the clear influence of Antarctic topography from the opposing anomalies on both sides of the AP; Strong positive response patterns are visible on the western side of the Antarctandes (mountain ridge over the AP), countered by negative response patterns on the eastern side. Contrary to the results from Sections 5.1 and 5.2, where the East Antarctic Ice Sheet and surrounding waters were dominated by negative temperature anomalies and positive SIC anomalies respectively, we observe a more alternating pattern of positive and negative precipitation anomalies over East Antarctica. Furthermore, we note that the largest response patterns are mostly concentrated at the coastal regions. This is a result that we expect since the Antarctic interior is a cold desert where large areas receive less than 10 mm total precipitation per season.

The Clausius-Clapeyron equation, which relates saturation vapor pressure to temperature, states that precipitation should increase by about 7% per 1°C increase (Ivancic and Shaw, 2016). ERA5 calculates the total precipitation averaged over the Antarctic continent at 40 mm per season, which is similar to the results found in literature (Vaughan et al., 1999). Based on these calculations, we expect a ∼3 mm increase in total precipitation per 1°C increase in temperature. Calculations obtained from Section 5.2 showed temperature decreases of ∼1 °C during autumn and winter, and ∼0.5 °C decreases during spring and summer. From the Clausius-Clapeyron relation, this would result in total precipitation decreases of 3 mm and 1.5 mm respectively. However, our results show precipitation increases of up to 5 mm in every season except autumn. This suggests that besides temperature, wind patterns play a dominant role in the impact on precipitation anomalies. Apart from causing a negative temperature response over East Antarctica, a strong ASL advects a larger amount of moist air towards the AIS, especially east of its central location, which is consistent with Figure 14. From the combined results of Section 5.2 and 5.3, we conclude that the negative temperature response on Antarctica as a consequence of a deep ASL is dominated by a strong SAM (large scale effect). Subsequently the more alternating patterns of positive and negative precipitation anomalies over East Antarctica are dominated by the surface wind patterns around the ASL (small scale effects). Hence, we do not expect a strong T-P relation according to Clausius-Clapeyron.

The precipitation anomalies observed in the ASL region, however, are similar to the temperature anomalies in , with positive anomalies in the eastern part and negative anomalies on the western side (ERA5). However, contrary to the stronger seasonal differences observed from Figure 13, we note much smaller seasonal differences from Figure 14. Temperature increases of ∼1°C for the ASL region during winter and spring coincide with precipitation increases of 23 and 38 mm respectively. During summer and autumn we observe both temperature and

precipitation decreases over the ASL region. Mostly, temperature and precipitation anomalies follow circulation patterns. Warm air is also more humid, so we would expect a correlation between temperature and precipitation on a smaller scale, such as the ASL region.

Variability in precipitation anomalies show similar patterns between CESM2 and ERA5. The alternation between positive and negative anomalies over East Antarctica from CESM2 shows a high degree of similarity with ERA5. Furthermore, we observe that local scale patterns such as the opposite patterns on both sides of the AP is also well simulated by CESM2. We note again, that the unrealistic location of large SLP anomalies over the Ross Sea during winter causes some model biases. While during most seasons we observe a clear distinction of positive response patterns in the eastern part and negative response patterns in the western part of the ASL region, this clear division of opposite anomalies is not visible during winter (Figure 14d). CESM2 calculates the T-P relation over the total AIS better than ERA5; negative precipitation anomalies (between -1 and -4 mm) over Antarctica are observed for every season, coinciding with the negative temperature anomalies (between -0.5°C and -1.5°C) that where found in Section 5.2.

In the next section, we will further examine this T-P relation with CESM2 for a future period.

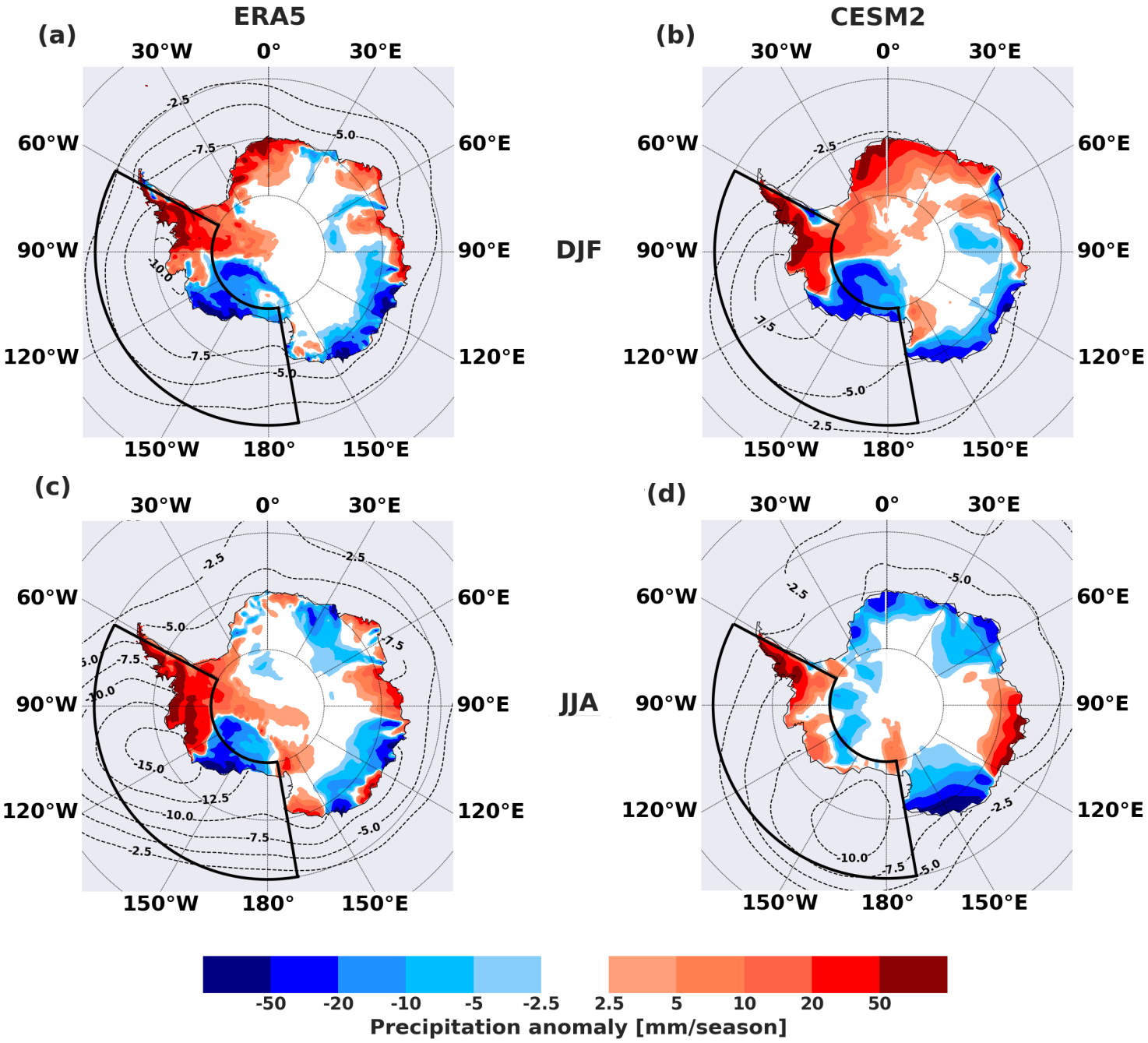

Figure 14: Total precipitation anomalies over Antarctica for the difference between strong (+ 1σ) and weak (- 1σ) ASL seasons. In the columns we vary the model, in the rows we vary the season. The black box shows the ASL region (60°-80° S, 170°-298° E) and the contour lines with intervals of 2.5 hPa display the anomalies in surface pressure over the Southern Ocean. Data from ERA5 and CESM2, 1979-2014.

6 Future projections

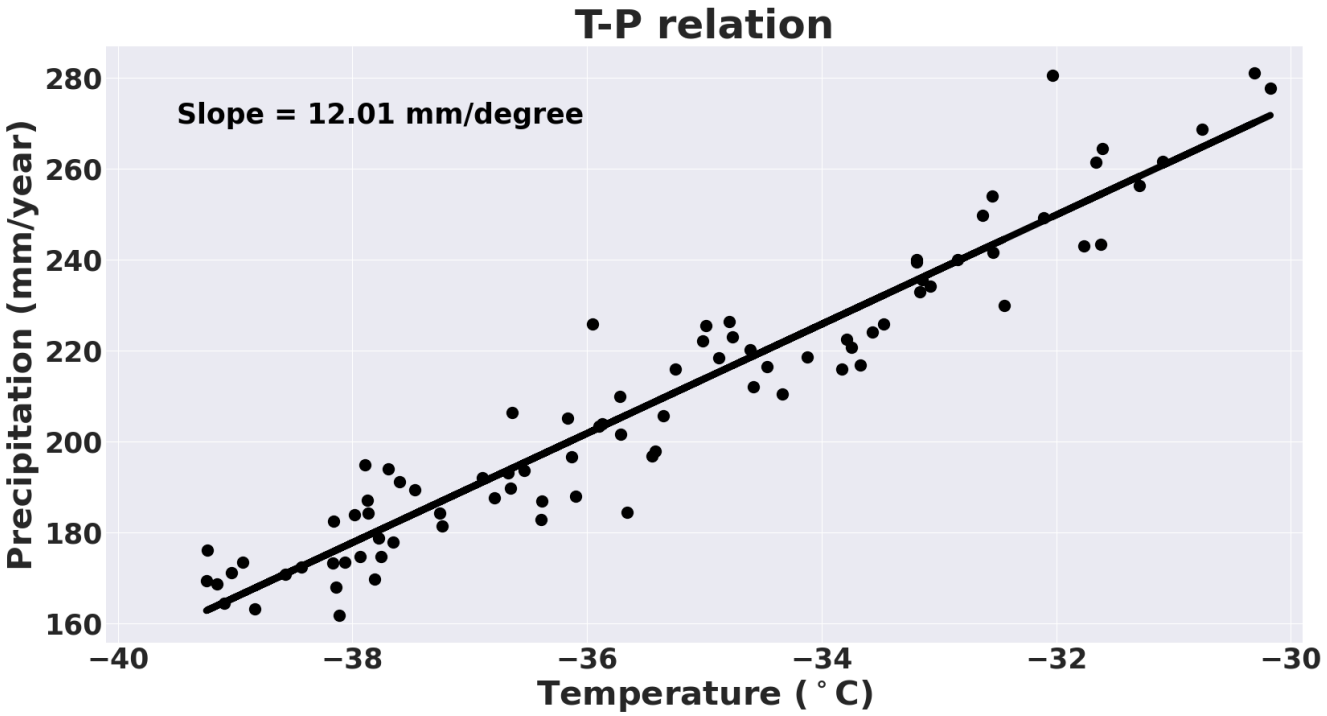

Figure 15: Relation between temperature (T) and precipitation (P) on Antarctica. Different dots represent one value per year for T and P for the period 2015-2100. The solid line represent the trend in T and P and the slope of the trend line is shown in the top left corner. Data from CESM2 SSP5-8.5, 2015-2100.

The relation between Temperature and Precipitation for the future period follows the expected pattern according to the Clausius-Clapeyron equation (Figure 15). Integrated over the total AIS, we calculate one value for precipitation and temperature for each year between 2015 and 2100. Using the SSP5-8.5 scenario, a temperature increase from -39 °C to -30 °C is modelled over Antarctica. Subsequently, we observe a precipitation increase from 160 to 270 mm/year. These increases in both temperature and precipitation over the AIS are strongly linked, suggested by the calculated correlation coefficient of more than 0.9 (significant at $p < 0.05$). The calculated slope measures an increase of 12 mm/°C, which represents a 7.5% increase in precipitation per degree increase in temperature, for a base precipitation level of 160 mm (i.e, $12/160 = 0.075$). This is very close to what is expected from Clausius Clapeyron, since the equation calculates an average slope of 7%. However, as the precipitation levels increase, the percentage of the slope decreases to 4.5% (i.e, $12/270 = 0.045$). This decreasing T-P slope with increasing temperature is a result that is corroborated with a previous study (Bürger et al., 2014). However, the amount of decrease (from 7.5% to 4.5%) is larger than expected. Besides the observed mean increase in temperature and precipitation over Antarctica, we find large regional differences, mainly owing to ASL deepening, which are further discussed below.

Future changes in the ASL are difficult to project because of its high variability in both depth and location on one hand, uncertainties in GHG concentrations and stratospheric ozone on the other (Goyal et al., 2021c; Hosking et al., 2016; Raphael et al., 2016). While increasing GHG concentrations and stratospheric ozone depletion had a exacerbating effect in strengthening of the SAM in the past, predictions are that the recovery of the ozone hole and further GHG

increase will have opposing effects in the future (Hosking et al., 2016). After stabilization of ozone recovery, expectations are that future changes in the SH mid-latitudes will be dominated by changes in GHG concentrations (Goyal et al., 2021c).

To assess future changes in the strength of the ASL and the SAM, we examine SLP values on the SH for the period 2015-2100 (SSP5-8.5 Scenario). Figure 16 shows the seasonal trends of the SLP field (units: hPa/decade) for this future period. We note a clear distinction between negative trends at high latitudes and predominantly positive trends at low and mid latitudes for all seasons. These opposing trends in surface pressure between mid and high latitudes are a reflection of the SAM becoming more positive, which is expected as a result of increasing GHG concentrations (Hosking et al., 2016). One would expect that the predicted Antarctic polar amplification and therefore the weaker SH meridional temperature gradient in the lower troposphere is associated with a weaker SAM. However, the projected rise in temperatures in the upper troposphere, which will increase faster over the equator than over the poles, intensifies the upper tropospheric meridional temperature gradient. As this is the main driver of the SAM, it causes the SAM to become more positive (Fogt and Marshall, 2020; Hosking et al., 2016; Masson-Delmotte et al., 2006). Besides intensification, we also note a poleward shift of the SAM, since the line of zero trend in Figure 16 is located southward from the line of zero SLP anomaly in Figure 8.

The anti-correlation between the ASL and SAM remains strong in a future climate, with values less than -0.7 (significant at $p < 0.05$) for all seasons. From Figure 16, we observe large seasonal differences in future intensification of the SAM and therefore seasonal differences in deepening of the ASL. Between 2015 and 2100, the largest reduction in ASL-SLP occurs during winter (up to 5 hPa), and the smallest during summer (around 2 hPa). Over the first half of the 21st century (2015-2060), we neither observe significant positive trends for the SAM during

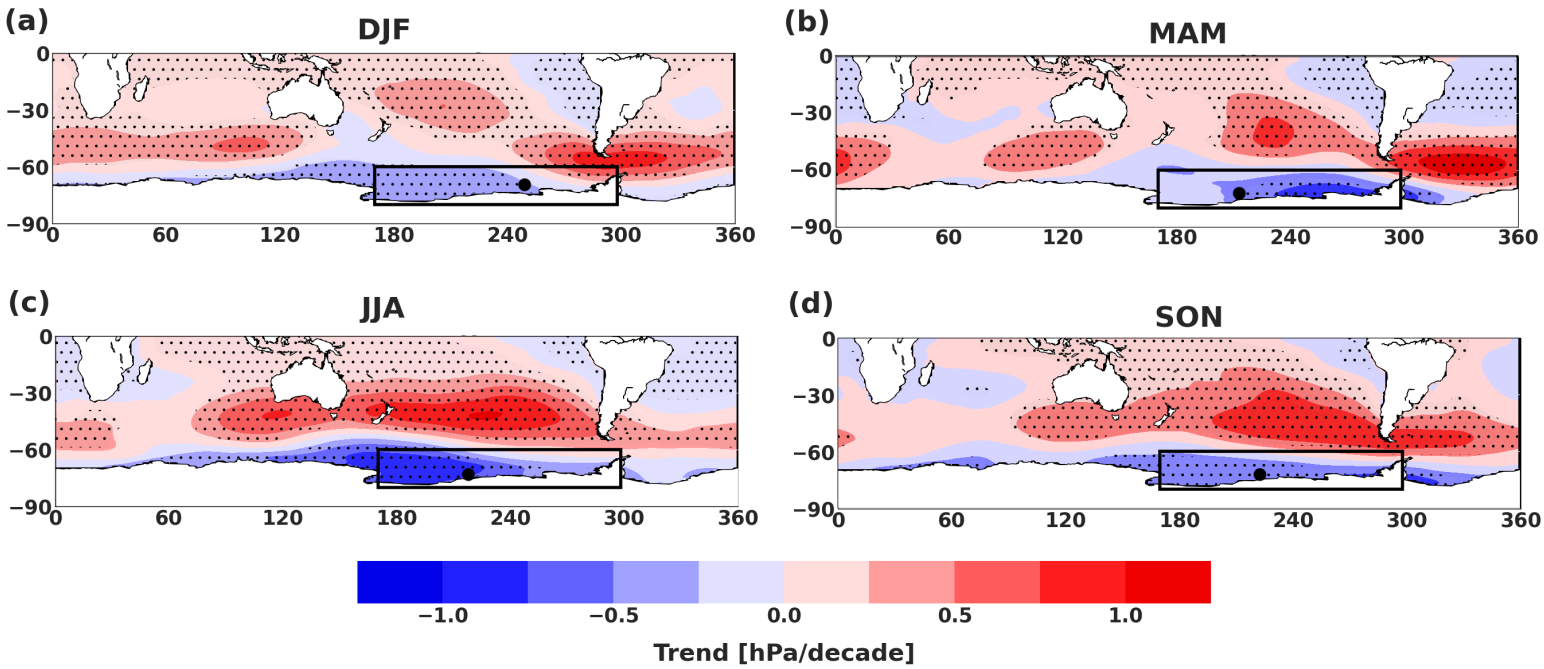

Figure 16: Trend in SLP on the SH in units of hPa/decade for (a): summer, (b): autumn, (c): winter and (d): spring. The ASL is defined in the black box, bounded by 60°-80° S and 170°-298° E. The large black dot represents the seasonal mean position of the ASL. The small black dots indicate where correlations are significant at the 95% confidence level. Data from CESM2 SSP5-8.5, 2015-2100.

summer and autumn nor a deepening ASL trend in summer. The recovery of the ozone hole over Antarctica is expected to oppose the SAM to become more positive during the first half of the 21st century (England et al., 2016; Raphael et al., 2016), therefore opposing ASL deepening trends as well. The ozone recovery has the largest effect during austral summer and to a lesser extent during autumn, which could be an explanation for the smaller trends observed during those seasons.

In the second half of the 21st century (2065-2100), however, the ASL undergoes significant deepening trends during every season. We note that strong ASL years (+ 1σ) occur more often towards the end of this period than weak ASL years (- 1σ). During winter and spring this background difference is largest and therefore we remove a 7 year trend in SIC, precipitation and temperature to compromise for these differences. During summer and autumn, a 2 year trend is removed. Figure 17 shows the resulting anomalies in SIC (a,b), temperature (c,d) and precipitation (e,f) for both summer (left) and winter (right), for which these trends are removed.

From Figure 17a,b we note that the amount of SIE is substantially reduced at the end of the 21st century, to less than half its seasonal extent compared to Figure 12. This is no surprise, due to the strong warming trend from the SSP5-8.5 scenario. The total SIE undergoes an even larger seasonal cycle compared to the current period (i.e., a four times larger spatial extent during winter than during summer). During summer, the sporadic amount of sea ice in the Southern Ocean is almost solely concentrated in the ASL region. Subsequently, we do not observe any sea ice around the coast of East Antarctica. We note predominantly negative SIC anomalies around the AIS during strong ASL years. Averaged over the total region surrounding Antarctica, we calculate the largest negative values during summer and autumn ($<$ -2%) and a smaller decrease in SIC during winter. These dominant negative responses are different from the result discussed in Section 5.1 where positive responses as a consequence of strong ASL years were dominating. CESM2 simulates similar SLP patterns for the summer season associated with strong ASL seasons in the future as for the present climate. This results in maximum values around 8 hPa in he ASL region. During winter (Figure 17b) we observe an increase in such SLP anomalies in the ASL region, while anomalies around East Antarctica are largely decreased to almost non existent. Variability in both SLP patterns and SIC patterns associated with ASL deepening suggest that there is a link between the two; during summer when SLP anomalies are smaller, we observe almost solely negative SIC anomalies, while in winter positive SIC anomalies exist over the Ross Sea, where southerly wind anomalies are larger.

The temperature anomalies shown in Figure 17c,d show large areas of a positive response over East Antarctica during strong ASL seasons, especially in summer. We did not observe these temperature increases in the current period analysis, where only negative temperature anomalies were observed over East Antarctica (Figure 13). Temperature calculations over the total AIS result in strong increases (around 1 °C) during summer and autumn as a response to ASL deepening. During winter and spring a small (between 0°C and 0.5°C) temperature decrease is found, which is significantly smaller than the temperature decreases from Section 5.2. Although we observe an average temperature decrease over the AIS during winter and spring, the large area (east of the AP) with positive patterns over East Antarctica, exists at that location throughout the year. This result suggests that ASL deepening results in a further spatial extent of surface wind patterns over parts of East Antarctica in the future, creating large areas of a warming response at locations where only negative temperature anomalies were found for the current climate.

The spatial patterns of precipitation anomalies (Figure 17e and f) show large similarities with the temperature anomalies (Figure 15c and d) for all seasons. Both summer and winter season show extensive areas of precipitation increases over East Antarctica during strong ASL years at roughly the same locations as temperature increases and vice versa. While from Figure 14, we observed a more alternating pattern of positive and negative anomalies over East Antarctica, Figure 17 shows large areas grouped together with either positive or negative precipitation anomalies. Calculations over the total AIS result in increasing precipitation for all seasons except winter. This result is consistent with the calculated values for seasonal temperature anomalies, which suggest that the T-P relation according to Clausius-Clapeyron is well simulated on a seasonal timescale as well (A strong relation that we already found on a yearly timescale from Figure15). The patterns in the ASL region show large similarities between all seasons, with precipitation increases at the eastern side and decreases in the west. We note that the strength of these anomalies correlates well with the strength of the SLP patterns, which is strongest during winter and weakest in summer.

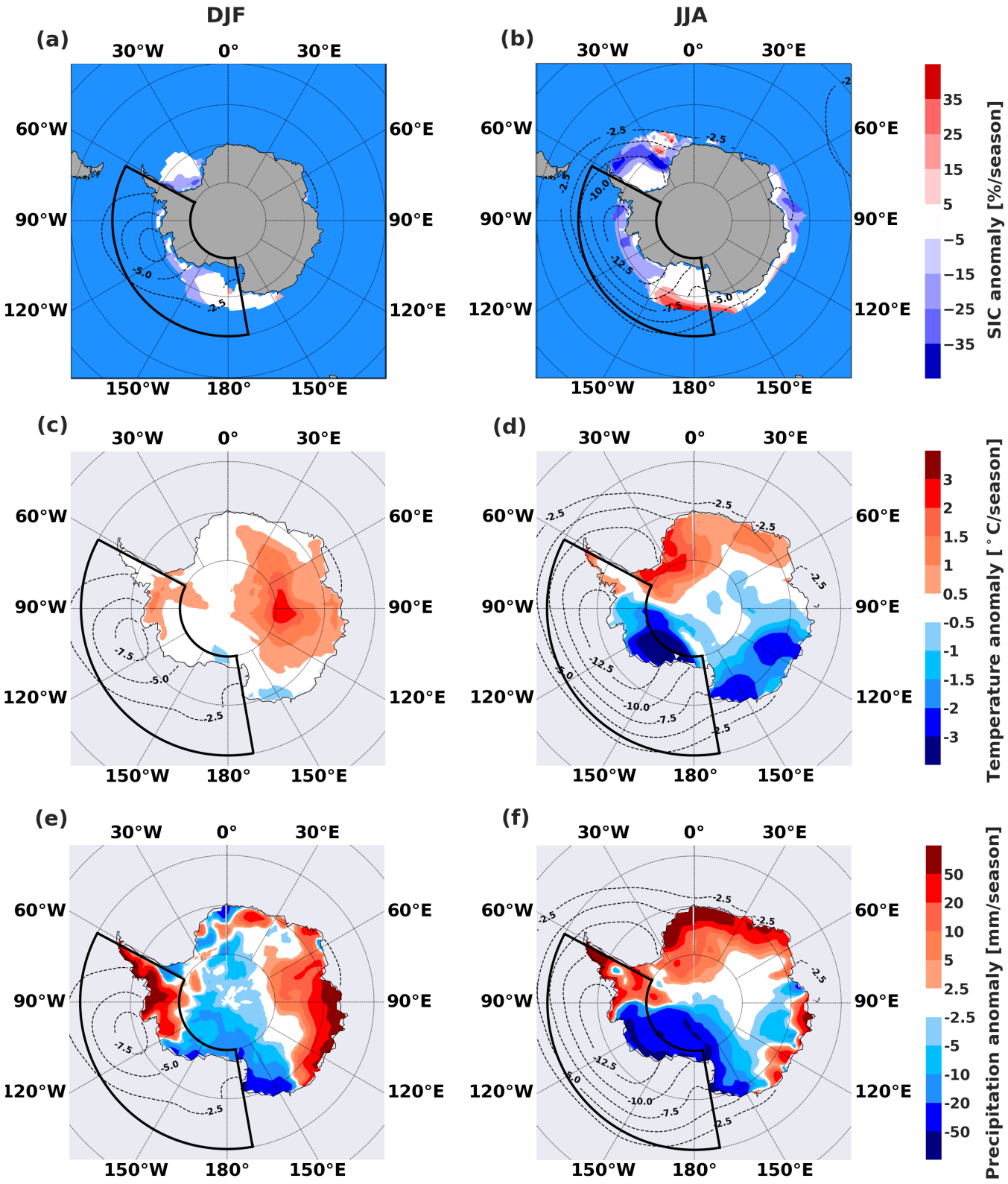

Figure 17: Seasonal anomalies in SIC (a,b), Temperature (c,d) and Precipitation (e,f) for the difference between strong (+ 1σ) and weak (- 1σ) ASL seasons. In the columns we vary the seasons. The black box shows the Amundsen Sea Low region (60°-80° S, 170°-298° E). Contour lines with intervals of 2.5 hPa display the anomalies in surface pressure over the Southern Ocean. Data from CESM2 SSP5-8.5, 2065-2100.

7 Summary and Conclusions

The aim of this research was to investigate the climatological ASL and its variability in current and future climates. A second aim was to study its impact on Antarctic SMB by examining the different patterns in sea ice, temperature and precipitation for strong and weak ASL years. We have studied the SLP climatology on monthly and seasonal timescales, which revealed that the ASL undergoes a zonal shift of more than 60° and a deepening of more than 10 hPa during its yearly cycle. Variability in depth is strongly influenced by the SAO, which results in the lowest SLP values around Antarctica during austral spring, due to the SAO's strongest contracted phase. Shifts in ASL location are firmly regulated by the mid-tropospheric planetary waves, as evidenced from the Z500 field. Analysis of the Z500 field reveals that the mid-tropospheric trough is stationed above the Ross Ice Shelf throughout the year. We observe the ASL's mean position slightly to the east of the upper level trough, which can be explained by the interaction with the westerly wind jet. During summer, a weaker meridional gradient in the Z500 field causes the ASL to shift further eastward towards the AP, explaining the large spatial variability in surface pressure in this area.

Using the high-quality ERA5-reanalysis dataset, we were able to create a consistent climatology for the ASL. However, the high degree of variability in both depth and location together with the relatively short period analysed (1979-2014) results in trends being insignificant, contrary to what was found in previous studies. When in those studies significant trends were found on even shorter timeseries, we conclude that those trends appeared by chance. This does not preclude, however, that if longer timeseries become available in the future, trends that were not significant in our analysis will become significant, especially when those trends are consistent with predictions based on theory.

The ASL is strongly influenced by the two largest modes of variability in the SH: SAM and ENSO. During the positive (negative) phase of the SAM, we observe larger (smaller)-than-normal pressure differences between the mid and high latitudes, often resulting in a deeper (weaker) ASL. The anti-correlations between the SAM and ASL are very high for every season ($\sim$-0.8), revealing the strong SAM influence throughout the year. Contrary to the SAM, the influence of ENSO events on pressure anomalies in the ASL region shows large seasonal differences. While we observe the largest areal extent of high correlations during summer, regression of SLP on ENSO temperature anomalies peaks during winter. The combined effects of the SAM and ENSO phases: SAM+ and La Nina, and SAM- and El Nino, result in large amplification of pressure anomalies (up to 6 hPa) in the ASL region, while other combinations show a reduced effect.

The ASL or the "pole of variability" is the main regulator in controlling surface winds in the Amundsen-Bellingshausen and Ross Seas and therefore has significant impact on West Antarctic and AP climate. SIC, temperature and precipitation over the AIS show marked patterns covarying with ASL-strength, especially affecting West Antarctica. In the ASL region, anomalies of both signs occur. On its eastern side, an anomalously deep ASL strengthens the northerly wind over the AP, transporting more relatively warm and moist air southward. On its western side relatively cold and dry air is carried northward over the Ross Sea. As a consequence of these surface wind anomalies, we detect a dominant pattern of negative (positive) SIC anomalies, combined with positive (negative) temperature and precipitation anomalies over the eastern (western) ASL region. The influence of ASL variability is not restricted to West Antarctica. Around the AIS, we find a dominant pattern of positive SIC anomalies combined with negative temperature and precipitation anomalies in most seasons. An anomalously deep ASL often simultaneously occurs with large pressure anomalies between

mid and high latitudes, causing a stronger zonal flow around Antarctica. This allows less penetration of relatively warm meridional surface winds from higher latitudes and therefore has a net cooling effect over the AIS, explaining the observed negative temperature anomalies.

In the ASL assessment for the current climate, we also assess the quality of CESM2 by comparing its output with ERA5. CESM2 underestimates surface pressures in the Southern Ocean by about 5-10 hPa, however, it captures the climatological seasonal differences adequately, with lowest SLP values during summer and highest during spring. Furthermore, the simulated location of the ASL showed a seasonal dependent model bias, especially during winter and spring. The links with SAM and ENSO show a high degree of similarity between CESM2 and ERA5. CESM2 is able to simulate the seasonality of the tropical teleconnection with ENSO adequately, which is a positive result. CESM2 underestimates the difference in SLP between strong (+ 1σ) and weak (- 1σ) ASL seasons. Since the strength of SLP anomalies in the ASL region is linked with the anomalies in SIC, temperature and precipitation over West Antarctica, these are underestimated as well. Besides CESM2 simulating local SLP differences in comparison to ERA5, the large scale anomaly patterns in SIC, temperature and precipitation over the AIS are similar, especially over East Antarctica.

We used the SSP5-8.5 scenario in CESM2 for our future analysis (2015-2100). The results showed that surface pressure around Antarctica will decrease in every season, causing the SAM to become more positive and the ASL to become deeper. The projected increase in GHG emissions plays a dominant role in the observed trends for the SAM and the ASL, which is expected to become deeper as a result of the stronger meridional temperature gradient in the upper troposphere. Projections for the period 2015-2100 show a deepening of the ASL up to 5 hPa during winter, with the lowest trend observed during summer ($\sim$2 hPa). These large seasonal differences have often been linked with the recovery of the ozone hole, which is a feature of austral spring, but has the largest impact during the subsequent season (austral summer). The stratospheric ozone increase, which is predicted to occur in the first half of the 21st century has an opposing effect on the ASL compared to the increase of GHG emissions, partly explaining the smaller observed trends in the ASL and SAM during summer. Another factor is the seasonal cycle in the SAM itself, which is much stronger in winter than in summer. Hence, an overall enhancement of the SAM is expected to be associated with stronger increases in winter than in summer.

Studying the influence of the ASL on the future climate of Antarctica, revealed interesting and opposing linkages compared to present-day climate. Our results showed that a stronger ASL caused predominantly positive SIC anomalies, together with temperature and precipitation decreases over Antarctica during the current period. However, examining an equal length future period (2065-2100) revealed that these dominant patterns were reduced and even showed opposing response patterns during some seasons. While the anomalies in the ASL region are approximately similar between current and future climates, large differences are observed over East Antarctica. Especially during summer and autumn we note that an abnormally strong ASL causes the area of a warming response on East Antarctica to increase, suggesting that the ASL will further spatially extent its influence on the Antarctic climate due to anthropogenic forcing. Furthermore, we observe a strong relation between temperature and precipitation over Antarctica in the future climate, in which the yearly total precipitation over the AIS increases between 4.5% and 7.5% per degree increase in temperature. We note this strong T-P relation on a seasonal timescale as well by the similar spatial patterns in Figure 17. Besides the projected ASL deepening, Hosking et al. (2016) showed that the ASL will likely move poleward and eastward in the future as a result of increasing GHG concentrations. This shift towards the AIS could be another explanation for the more dominant impact of the ASL on the future East

Antarctic climate.

Our tentative explanation for the opposing SIC, temperature and precipitation responses on ASL deepening in future and present day climate is that they result as the net effect of two counteracting mechanisms. The cooling response is associated with a stronger SAM that further isolates the Antarctic continent from the SH subtropics. The warming response is associated with a stronger ASL that enhances exchange with the Southern Ocean. We hypothesize that the isolating effect by a stronger SAM saturates and becomes weaker in the future, while exchange with a warmer Southern Ocean becomes more prominent as sea ice extent decreases.

8 Limitations and directions for future research

One of the limitations in conducting the analysis of the ASL during the current climate was the relatively short period of the ERA5-reanalysis dataset (1979-2014). Although we could have expanded this period with 6 years (1979-2020), this would cause biases in our comparison with CESM2, for which the historical period ends in 2014. Although the preliminary dataset for ERA5 (1950-1978) is available on the SH as well, the quality of this dataset decreases drastically compared to the contemporary reanalysis (Bell et al., 2021).

A logical next step for further examination of the ASL could be extending the period of analysis by using the NCEP/NCAR reanalysis 1 product (1948-present) (Compo et al., 2008) or the 20th century reanalysis product from the NOAA (1836-2015) (Compo et al., 2011). Although these products are coarser-gridded than the ERA5-reanalysis from ECMWF used in this study, these longer time periods could provide further insights in past variability of the ASL and especially trends.

For our future analysis, we used model results from one member of CESM2. Although we validated that this member is a good representation of a multi-member mean (using 3 members), a more robust result would have been obtained if all members were used (due to time limitations we only used 3). Furthermore, it would be interesting to see how model dependent our results are and to this end a similar analysis with the multimodel ensemble-mean of CMIP6 could be performed.

The central position of the ASL was derived by finding the grid cell with the lowest value of SLP within the box bounded by 60°-80° S, 170°-298° E. Minima outside this box were not counted in our definition of the ASL. Although the choice of Antarctic orographic features as boundaries for our ASL box was based on various previous studies (Hosking et al., 2016; Goyal et al., 2021b), this choice is not unambiguous in the literature. It would be interesting to assess whether our results are sensitive to the exact definition of the ASL box.

The ASL has a large influence on the West Antarctic Ice Sheet with the potential to accelerate future ice-loss and thereby contributing to global sea-level rise. Despite this the ASL has been the central subject of relatively few studies and is still not completely understood. Questions that remain unanswered are: What is the impact of different weather systems on the ASL? What was the role of the ASL during past climates? Why does the ASL extent its spatial influence on East Antarctica due to anthropogenic forcing? Also, the role of the ASL in regulating the upwelling of Circumpolar Deep Water onto the Antarctic continental shelves needs to be further examined. We recommend that future research will focus on answering these questions, as well as making efforts to better understand the influence of the other two climatological low pressure systems around Antarctica on its climate.

References

Bell, B., Hersbach, H., Simmons, A., Berrisford, P., Dahlgren, P., Horányi, A., Muñoz-Sabater, J., Nicolas, J., Radu, R., Schepers, D., et al. (2021). The era5 global reanalysis: Preliminary extension to 1950. *Quarterly Journal of the Royal Meteorological Society*.

Bürger, G., Heistermann, M., and Bronstert, A. (2014). Towards subdaily rainfall disaggregation via clausius–clapeyron. *Journal of Hydrometeorology*, 15(3):1303–1311.

Clem, K. R., Renwick, J. A., and McGregor, J. (2017). Large-scale forcing of the amundsen sea low and its influence on sea ice and west antarctic temperature. *Journal of Climate*, 30(20):8405–8424.

Coggins, J. H. and McDonald, A. J. (2015). The influence of the amundsen sea low on the winds in the ross sea and surroundings: Insights from a synoptic climatology. *Journal of Geophysical Research: Atmospheres*, 120(6):2167–2189.

Cohen, L., Dean, S., and Renwick, J. (2013). Synoptic weather types for the ross sea region, antarctica. *Journal of climate*, 26(2):636–649.

Compo, G. P., Whitaker, J. S., and Sardeshmukh, P. D. (2008). The 20th century reanalysis project. In *Proc. Third WCRP Int. Conf. on Reanalysis*.

Compo, G. P., Whitaker, J. S., Sardeshmukh, P. D., Matsui, N., Allan, R. J., Yin, X., Gleason, B. E., Vose, R. S., Rutledge, G., Bessemoulin, P., et al. (2011). The twentieth century reanalysis project. *Quarterly Journal of the Royal Meteorological Society*, 137(654):1–28.

Danabasoglu, G., Lamarque, J.-F., Bacmeister, J., Bailey, D., DuVivier, A., Edwards, J., Emmons, L., Fasullo, J., Garcia, R., Gettelman, A., et al. (2020). The community earth system model version 2 (cesm2). *Journal of Advances in Modeling Earth Systems*, 12(2).

Ding, Q., Wallace, J. M., Battisti, D. S., Steig, E. J., Gallant, A. J., Kim, H.-J., and Geng, L. (2014). Tropical forcing of the recent rapid arctic warming in northeastern canada and greenland. *Nature*, 509(7499):209–212.

Ebi, K. L., Hallegatte, S., Kram, T., Arnell, N. W., Carter, T. R., Edmonds, J., Kriegler, E., Mathur, R., O'Neill, B. C., Riahi, K., et al. (2014). A new scenario framework for climate change research: background, process, and future directions. *Climatic Change*, 122(3):363–372.

England, M. R., Polvani, L. M., Smith, K. L., Landrum, L., and Holland, M. M. (2016). Robust response of the amundsen sea low to stratospheric ozone depletion. *Geophysical Research Letters*, 43(15):8207–8213.

Fogt, R. L. and Marshall, G. J. (2020). The southern annular mode: Variability, trends, and climate impacts across the southern hemisphere. *Wiley Interdisciplinary Reviews: Climate Change*, 11(4):e652.

Fogt, R. L., Wovrosh, A. J., Langen, R. A., and Simmonds, I. (2012). The characteristic variability and connection to the underlying synoptic activity of the amundsen-bellingshausen seas low. *Journal of Geophysical Research: Atmospheres*, 117(D7).

Fogt, R. L. and Zbacnik, E. A. (2014). Sensitivity of the amundsen sea low to stratospheric ozone depletion. *Journal of Climate*, 27(24):9383–9400.

Glantz, M. H. and Ramirez, I. J. (2020). Reviewing the oceanic niño index (oni) to enhance societal readiness for el niño's impacts. *International Journal of Disaster Risk Science*, 11:394–403.

Gong, D. and Wang, S. (1999). Definition of antarctic oscillation index. *Geophysical research letters*, 26(4):459–462.

Goyal, R., Jucker, M., Gupta, A. S., Hendon, H., and England, M. (2021a). Zonal wave 3 pattern in the southern hemisphere generated by tropical convection.

Goyal, R., Jucker, M., Sen Gupta, A., and England, M. H. (2021b). Generation of the amundsen sea low by antarctic orography. *Geophysical Research Letters*, 48(4):e2020GL091487.

Goyal, R., Sen Gupta, A., Jucker, M., and England, M. H. (2021c). Historical and projected changes in the southern hemisphere surface westerlies. *Geophysical Research Letters*, 48(4):e2020GL090849.

Hersbach, H., Bell, B., Berrisford, P., Hirahara, S., Horányi, A., Muñoz-Sabater, J., Nicolas, J., Peubey, C., Radu, R., Schepers, D., et al. (2020). The era5 global reanalysis. *Quarterly Journal of the Royal Meteorological Society*, 146(730):1999–2049.

Hosking, J. S., Orr, A., Bracegirdle, T. J., and Turner, J. (2016). Future circulation changes off west antarctica: Sensitivity of the amundsen sea low to projected anthropogenic forcing. *Geophysical Research Letters*, 43(1):367–376.

Hosking, J. S., Orr, A., Marshall, G. J., Turner, J., and Phillips, T. (2013). The influence of the amundsen–bellingshausen seas low on the climate of west antarctica and its representation in coupled climate model simulations. *Journal of Climate*, 26(17):6633–6648.

Ivancic, T. J. and Shaw, S. B. (2016). A us-based analysis of the ability of the clausius-clapeyron relationship to explain changes in extreme rainfall with changing temperature. *Journal of Geophysical Research: Atmospheres*, 121(7):3066–3078.

Lachlan-Cope, T. A., Connolley, W. M., and Turner, J. (2001). The role of the non-axisymmetric antarctic orography in forcing the observed pattern of variability of the antarctic climate. *Geophysical research letters*, 28(21):4111–4114.

Lenaerts, J. T., Van Den Broeke, M. R., Scarchilli, C., and Agosta, C. (2012). Impact of model resolution on simulated wind, drifting snow and surface mass balance in terre adélie, east antarctica. *Journal of Glaciology*, 58(211):821–829.

Maclennan, M. L. and Lenaerts, J. T. (2021). Large-scale atmospheric drivers of snowfall over thwaites glacier, antarctica. *Geophysical Research Letters*, 48(17):e2021GL093644.

Marshall, G. J. (2003). Trends in the southern annular mode from observations and reanalyses. *Journal of climate*, 16(24):4134–4143.

Masson-Delmotte, V., Kageyama, M., Braconnot, P., Charbit, S., Krinner, G., Ritz, C., Guilyardi, E., Jouzel, J., Abe-Ouchi, A., Crucifix, M., et al. (2006). Past and future polar amplification of climate change: climate model intercomparisons and ice-core constraints. *Climate Dynamics*, 26(5):513–529.

Pope, J. O., Holland, P. R., Orr, A., Marshall, G. J., and Phillips, T. (2017). The impacts of el niño on the observed sea ice budget of west antarctica. *Geophysical Research Letters*, 44(12):6200–6208.

Raphael, M. (2004). A zonal wave 3 index for the southern hemisphere. *Geophysical Research Letters*, 31(23).

Raphael, M. N. and Hobbs, W. (2014). The influence of the large-scale atmospheric circulation on antarctic sea ice during ice advance and retreat seasons. *Geophysical Research Letters*, 41(14):5037–5045.

Raphael, M. N., Marshall, G., Turner, J., Fogt, R., Schneider, D., Dixon, D., Hosking, J., Jones, J., and Hobbs, W. R. (2016). The amundsen sea low: Variability, change, and impact on antarctic climate. *Bulletin of the American Meteorological Society*, 97(1):111–121.

Scott Yiu, Y. Y. and Maycock, A. C. (2019). On the seasonality of the el niño teleconnection to the amundsen sea region. *Journal of Climate*, 32(15):4829–4845.

Tetzner, D., Thomas, E., and Allen, C. (2019). A validation of era5 reanalysis data in the southern antarctic peninsula—ellsworth land region, and its implications for ice core studies. *Geosciences*, 9(7):289.

Timmermann, A., An, S.-I., Kug, J.-S., Jin, F.-F., Cai, W., Capotondi, A., Cobb, K. M., Lengaigne, M., McPhaden, M. J., Stuecker, M. F., et al. (2018). El niño–southern oscillation complexity. *Nature*, 559(7715):535–545.

Turner, J., Hosking, J. S., Marshall, G. J., Phillips, T., and Bracegirdle, T. J. (2016). Antarctic sea ice increase consistent with intrinsic variability of the amundsen sea low. *Climate Dynamics*, 46(7-8):2391–2402.

Turner, J., Phillips, T., Hosking, J. S., Marshall, G. J., and Orr, A. (2013). The amundsen sea low. *International Journal of Climatology*, 33(7):1818–1829.

Van den Broeke, M. (2000). The semiannual oscillation and antarctic climate, part 5: impact on the annual temperature cycle as derived from ncep/ncar re-analysis. *Climate dynamics*, 16(5):369–377.

Van Wessem, J., Reijmer, C., Morlighem, M., Mouginot, J., Rignot, E., Medley, B., Joughin, I., Wouters, B., Depoorter, M., Bamber, J., et al. (2014). Improved representation of east antarctic surface mass balance in a regional atmospheric climate model. *Journal of Glaciology*, 60(222):761–770.

Vaughan, D. G., Bamber, J. L., Giovinetto, M., Russell, J., and Cooper, A. P. R. (1999). Reassessment of net surface mass balance in antarctica. *Journal of climate*, 12(4):933–946.

Visbeck, M. (2009). A station-based southern annular mode index from 1884 to 2005. *Journal of Climate*, 22(4):940–950.

Yuan, X. and Li, C. (2008). Climate modes in southern high latitudes and their impacts on antarctic sea ice. *Journal of Geophysical Research: Oceans*, 113(C6).

Zhu, J., Xie, A., Qin, X., Wang, Y., Xu, B., and Wang, Y. (2021). An assessment of era5 reanalysis for antarctic near-surface air temperature. *Atmosphere*, 12(2):217.